SLAC-PUB-5796
April 1992
T/A

# ITERATIVE DETERMINATION OF INVARIANT TORI FOR TIME-PERIODIC HAMILTONIAN WITH TWO DEGREES OF FREEDOM*†

W. E. GABELLA‡

*Department of Physics, University of Colorado, Boulder, Colorado 84309*

*and Stanford Linear Accelerator Center, Stanford University, Stanford, California 94309*

R. D. RUTH AND R. L. WARNOCK

*Stanford Linear Accelerator Center, Stanford University, Stanford, California 94309*

## ABSTRACT

We describe a nonperturbative numerical technique for solving the Hamilton-Jacobi equation of a nonlinear Hamiltonian system. We find the time-periodic solutions which yield accurate approximations to invariant tori. The method is suited to the case in which the perturbation to the underlying integrable system has a periodic and not necessarily smooth dependence on the time. This case is important in accelerator theory, where the perturbation is a periodic step function in time. The Hamilton-Jacobi equation is approximated by its finite-dimensional Fourier projection with respect to angle variables, then solved by Newton's method. To avoid Fourier analysis in time, which is not appropriate in the presence of step functions, we enforce time-periodicity of solutions by a shooting algorithm. The method is tested in soluble models, and finally applied to a non-integrable example, the transverse oscillations of a particle beam in a storage ring, in two degrees of

* Work supported by the Department of Energy, contracts DE–AC03–76SF00515 and DE–FG02–86ER40302.

† Submitted to Physical Review A.

‡ Currently visiting Fermilab MS345, P.O.Box 500, Batavia, IL, 60510, from University of California, Los Angeles.

Submitted to *Physical Review A.*

freedom. In view of the time dependence of the Hamiltonian, this is a case with "2 1/2 degrees of freedom", in which phenomena like Arnol'd Diffusion can occur.

# I. INTRODUCTION

Examples of nonlinear Hamiltonian systems abound in applications of classical and semi-classical mechanics: the problem of N bodies interacting via gravitational or electromagnetic forces, the beam-beam interaction in storage rings with colliding beams, and the control of magnetic field configurations in plasma containment devices, to name but a few. Most of these problems are not soluble by quadratures and not completely integrable in the technical sense of the Liouville-Arnol'd theorem.[1] Interesting examples of completely integrable systems have been studied intensely, but they are essentially different from generic problems of nonlinear mechanics.[2]

We are concerned with systems that may be viewed as perturbed integrable systems. If the perturbation is sufficiently small, and the unperturbed Hamiltonian satisfies a non-degeneracy condition, the Kolmogorov-Arnol'd-Moser (KAM) theorem may apply.[3] The unperturbed system has toroidal surfaces in phase space that are invariant under time evolution, and these tori foliate the space. That is, the trajectory passing through any point in phase space lies on an invariant torus. The KAM theorem asserts that certain of these tori, those that have rationally independent perturbed frequencies, survive in a slightly distorted form when a sufficiently weak perturbation is imposed. These are called KAM tori; they form a set of large measure, but they are interleaved by regions in which tori need not exist, the so-called resonant regions of phase space corresponding to rationally dependent

unperturbed frequencies. Resonances exist in an arbitrarily small neighborhood of a KAM torus, so that the tori no longer foliate phase space.

For systems of sufficiently small phase space dimension, the existence of invariant tori has a direct implication for stability of the motion. The effective dimension of phase space is $D = 2d + \tau$, where $d$ is the number of mechanical degrees of freedom, and $\tau = 0$ for an autonomous system, while $\tau = 1$ if the Hamiltonian depends periodically on the time; (we exclude non-periodic time dependence). If $D \leq 4$ an invariant torus divides the space into two disjoint regions, an inside and an outside. It is clear that an orbit beginning inside the torus must stay there forever. This amounts to a useful statement of stability, if the inside is a bounded domain representing a desirable region of phase space for the problem at hand.

If $D > 4$, the KAM tori have too few dimensions to separate regions of phase space, just as a point does not divide a two-dimensional plane into disjoint regions. In this event, an orbit initially close to an invariant torus (though not on one) can follow a "stochastic web" associated with resonances, and eventually deviate greatly from the torus. Such an effect was demonstrated by Arnol'd in an example with $D = 5$, and similar phenomena are referred to broadly as Arnol'd Diffusion.[4]

For the study of stability of nonintegrable systems, it is useful to compute approximations to invariant tori, even in cases with $D > 4$. In contrast to exact invariant tori, a family of approximate invariant tori, corresponding to various values of an approximately invariant action, may foliate a region of phase space. Such a family is equivalent to a canonical transformation to new action-angle variables, such that the action is an approximate invariant. By studying the relatively weak variation in time of the new action, one can set bounds on the motion for a long

but finite time.[6] This argument is in the spirit of the Nekhoroshev Theorem[7], and proceeds in the same way for any $D$.

In a less formal way, a nearly invariant torus is useful in giving information on the dominant resonances. When the torus is represented as a Fourier series in angle variables, the magnitude of the Fourier coefficient in a particular mode measures the strength of excitation of a resonance in that mode. Also, the derivatives of the Fourier coefficients with respect to action, which determine the Jacobian of the transformation of angle variables in an associated canonical transform, have been identified as a sensitive indicator of the onset of large-scale chaos, at least for a class of models[5] with $D = 3$. Generally speaking, a difficulty in finding good approximate invariants is associated with the approach to strongly unstable regions, and for that reason it is informative to see what happens to good invariants as some measure of nonlinearity is increased.

Perturbative methods to compute approximate invariant tori have been employed over many decades. Since the advent of the computer, one tendency has been to adapt and improve classical perturbative algorithms for machine calculation, so as to carry the perturbation series to relatively high orders. Another tendency has been to invent non-perturbative techniques, again taking advantage of computers. Even with the power of computer implementations, perturbative methods may be ineffective in interesting parts of phase space, particularly near the onset of strong instability. Appropriate non-perturbative methods may have a larger region of validity, and even present some advantages in cases for which perturbation theory is adequate.

This paper describes a particular nonperturbative technique,[8,9] based upon iterative solution of the Hamilton-Jacobi equation. The method is designed to handle a Hamiltonian with periodic time dependence, allowing for the possibility that the time dependence may not be smooth. Following the pattern of canonical perturbation theory, the technique makes use of the action-angle variables of the underlying integrable system, and finds a transformation to new action-angle variables so that the new action is nearly constant. The generator of this transformation, an approximate solution of the Hamilton-Jacobi equation, provides an explicit representation of a nearly invariant torus.

The generator is represented as a finite Fourier series in angle coordinates. Departing from the method first used in iterative solution of the Hamilton-Jacobi equation,[5] we avoid Fourier analysis in time. Since the perturbations of present interest are discontinuous functions of time, a Fourier analysis would be inefficient and poorly convergent. Lacking the automatic periodicity of Fourier analysis, we enforce periodicity of the generator in time by a "shooting method" in which initial conditions are varied systematically until periodicity is achieved.

We illustrate the procedure with examples from accelerator theory with $D = 3$ and $D = 5$. The examples deal with oscillations of particles transverse to the direction of the beam, the so-called betatron oscillations. Nonlinearity of the motion arises from fields of sextupole magnets, which are introduced to counteract dependence of the oscillation frequencies on the longitudinal momentum of the beam. In these examples the method has a large domain of convergence, including regions of strong nonlinearity. It produces close approximations to invariant tori; this is checked by following single orbits, originating on the tori, through accurate

numerical integration of the equations of motion.

A comparison to related work requires some awareness of technical features of our approach; for that reason we defer comparisons to the final section of the paper.

In Section II, we derive the Fourier projection of the Hamilton-Jacobi equation in a form suitable for the shooting algorithm. The shooting method is formulated as a fixed-point problem in Section III. Iterative, numerical methods used to solve the fixed-point problem are briefly discussed. In Section IV, the technique is tested on two soluble examples. In Section V, the method is applied to a nontrivial example, the problem of betatron oscillations in a model of an accelerator with strong nonlinearities. Calculations of tori for both $D = 3$ and $D = 5$ are discussed. We give conclusions and try to place the method in a context of related work in Section VI. Appendix I contains a proof of convergence of the shooting algorithm for sufficiently weak nonlinearities, based on the contraction mapping theorem.

## II. FINITE FOURIER PROJECTION OF THE HAMILTON-JACOBI EQUATION

In this section we derive the projected Hamilton-Jacobi equation for charged particle motion in a transverse magnetic field. The discussion is applicable, however, to any time-periodic Hamiltonian representing a perturbed integrable system. We write the Hamiltonian in the action-angle variables of the integrable part and describe the time-periodic canonical transformation to the action-angle variables of the entire, nonlinear Hamiltonian. The equation requiring that the new Hamiltonian be independent of angles is the Hamilton-Jacobi equation, a partial differential

equation for the generating function of the transformation. We project it onto a finite Fourier basis in the angle variable and find a set of equations and boundary conditions for the Fourier amplitudes of the generator.

For a single charged particle moving in the static, transverse magnetic field of a cyclic ("circular") accelerator or storage ring, the Hamiltonian describing the transverse motion can be written in the action-angle variables of the unperturbed (linear) Hamiltonian as[10]

$$H(\mathbf{\Phi}, \mathbf{I}, s) = \mathbf{\Omega}(s) \cdot \mathbf{I} + V(\mathbf{\Phi}, \mathbf{I}, s) \quad . \tag{1}$$

The time-like variable $s$ is the independent variable of Hamilton's equations; it represents the particle's azimuthal location in the accelerator, measured by arc length along a closed reference orbit of circumference $C$. Boldface characters indicate $d$-component vectors, where $d = 1$ or $d = 2$ in all of our numerical examples. For $d = 2$ each component of any vector corresponds to one of the directions transverse to the reference orbit. The unperturbed Hamiltonian, $\mathbf{\Omega}(s) \cdot \mathbf{I}$, is defined in terms of $\beta_i(s) = 1/\Omega_i(s)$, where $\beta_i$ is the Courant-Snyder beta function which characterizes entirely the linear aspects of the applied magnetic fields.[11] Both $\beta_i$ and the perturbation $V$ are periodic in $s$ with period $C$.

The Hamiltonian (1) is derived from an initial formulation in terms of phase-space coordinates $(x_i, p_i)$, where $x_i$ is the transverse displacement of the particle from the reference orbit, and $p_i = dx_i/ds$. These coordinates are related to the unperturbed angle-action variables $(\Phi_i, I_i)$ by a canonical transformation,

$$x_i = \sqrt{2I_i\beta_i(s)} \quad \cos\Phi_i \quad ,$$
$$p_i = -\sqrt{2I_i/\beta_i(s)} \quad (\sin\Phi_i + \alpha_i(s)\cos\Phi_i) \ , \quad i = 1,2 \ , \tag{2}$$

where $2\alpha_i(s) = -d\beta_i(s)/ds$. In terms of $(x_i, p_i)$, the unperturbed Hamiltonian takes the form

$$H = \sum_{i=1}^{2} [\frac{p_i^2}{2} + K_i(s)\frac{x_i^2}{2}] \quad , \tag{3}$$

where the functions $K_i(s)$, periodic with period $C$, describe linear focusing forces from quadrupole magnets. The definition of $K_i$ and the determination of $\beta_i$ from $K_i$ is explained in Ref. 10.

When $V = 0$ the motion is integrable, since it follows immediately from Hamilton's equations that $I_i$ is constant, and that $\Phi_i(s) = \Phi_i(0) + \int_0^s d\sigma/\beta_i(\sigma)$. With $V = 0$ it is possible to make a further canonical transformation to variables that represent simple harmonic motion, but it is not convenient to do so in the following work.

Synchrotron oscillations and synchrotron radiation of the particle are ignored. Synchrotron oscillations (oscillations in energy associated with the electric r.f. accelerating field) occur on a time scale much longer than the betatron (transverse) oscillation time. They can have an important effect on long-term stability, but lead to a more complicated problem than the one we wish to study here. Synchrotron radiation tends to damp the betatron oscillations in electron accelerators, and in fact improves stability.

The form of $V$ for a string of normal sextupole magnets distributed about the

circumference of the ring is

$$V(x_1, x_2, s) = \sum_{n=1}^{N} f_n(s) \frac{S_n}{3!}(x_1^3 - 3x_1 x_2^2) \quad . \tag{4}$$

The function $f_n(s)$ is zero everywhere except inside the $n$-th magnet where it is unity. The sextupole strength $S_n$ has units of $\mathrm{m}^{-3}$, and is defined as $S = (e/cp_0)\,\partial^2 B_2/\partial x_1^2$ in cgs units, where $p_0$ is the reference momentum, and the second derivative of the vertical magnetic field $B_2$ is evaluated at $x_1 = x_2 = 0$.

We now consider the full nonlinear problem and seek a canonical transformation to new action-angle variables,[12]

$$(\mathbf{\Phi}, \mathbf{I}) \rightarrow (\mathbf{\Psi}, \mathbf{J}) \quad , \tag{5}$$

such that the new action $\mathbf{J}$ is invariant. The generating function of the transformation is denoted as

$$F_2(\mathbf{\Phi}, \mathbf{J}, s) = \mathbf{\Phi} \cdot \mathbf{J} + G(\mathbf{\Phi}, \mathbf{J}, s) \quad , \tag{6}$$

where the first term represents the identity map. The equations defining the transformation are

$$\mathbf{\Psi} = \mathbf{\Phi} + G_{\mathbf{J}}(\mathbf{\Phi}, \mathbf{J}, s) \quad , \tag{7}$$

$$\mathbf{I} = \mathbf{J} + G_{\mathbf{\Phi}}(\mathbf{\Phi}, \mathbf{J}, s) \quad , \tag{8}$$

$$H_1(\mathbf{J}, \mathbf{\Psi}, s) = H(\mathbf{\Phi}, \mathbf{J} + G_{\mathbf{\Phi}}, s) + G_s \quad . \tag{9}$$

The subscripts represent partial differentiation, for instance $G_{\mathbf{\Phi}} = \{\partial G/\partial \Phi_i\}$. The Hamilton-Jacobi equation expresses the requirement that the new Hamiltonian be a function of $\mathbf{J}$ and $s$ alone:

$$H_1(\mathbf{J}, s) = \mathbf{\Omega}(s) \cdot (\mathbf{J} + G_{\mathbf{\Phi}}) + V(\mathbf{\Phi}, \mathbf{J} + G_{\mathbf{\Phi}}, s) + G_s \quad . \tag{10}$$

If $G$ satisfies this partial differential equation, then $\mathbf{J}$ is invariant, as a direct result of Hamilton's equations in the new variables.

We seek a solution $G$ of Eqn. (10) that is periodic in $\mathbf{\Phi}$ with period $2\pi$, and periodic in $s$ with period $C$. Such a solution provides an explicit representation of a $(d+1)$-dimensional invariant torus, through Eqn. (8). Since $\mathbf{J}$ will be constant along an orbit $(\mathbf{\Phi}(s), \mathbf{I}(s))$, all points of the orbit lie on the surface $\mathbf{I} = \mathbf{I}(\mathbf{\Phi}, s; \mathbf{J})$ specified by Eqn. (8). The surface is toroidal, which means that $\mathbf{I}(\mathbf{\Phi}, s)$ is periodic in $\mathbf{\Phi}$ and $s$. The value of the constant vector $\mathbf{J}$ serves to distinguish different tori. Since only approximate solutions of (10) can be achieved numerically, our computations will lead to tori and actions $\mathbf{J}$ that are invariant only to a certain accuracy, as verified over a finite interval of $s$.

Because of the periodicity in the angles, it is natural to study Eqn. (10) in a Fourier basis in $\mathbf{\Phi}$. Accordingly, we expand the generator in a finite Fourier series, thus guaranteeing periodicity in $\mathbf{\Phi}$:

$$G(\mathbf{\Phi}, \mathbf{J}, s) = g(\mathbf{0}, \mathbf{J}, s) + \sum_{\mathbf{m} \in M \cup \bar{M}} g(\mathbf{m}, \mathbf{J}, s) e^{i\mathbf{m}\cdot\mathbf{\Phi}} \quad , \tag{11}$$

$$g(\mathbf{m}, \mathbf{J}, s) = \int_0^{2\pi} \frac{d\mathbf{\Phi}}{(2\pi)^d} e^{-i\mathbf{m}\cdot\mathbf{\Phi}} G(\mathbf{\Phi}, \mathbf{J}, s) \quad . \tag{12}$$

In Eqn.(11), the mode index vector $\mathbf{m} = (m_1, m_2, \ldots, m_d)$ runs over a finite set denoted as $M \cup \bar{M}$, which does not include $\mathbf{m} = (0, 0, \ldots, 0)$.

The set of indices for the independent, complex Fourier modes is $M$. The set $\bar{M}$ is simply related to $M$ and represents Fourier modes that are not independent of those with indices in $M$. In the case $d = 2$, the set $M$ is the set of all integer vectors $(m_1, m_2)$ such that $m_1 \in [0, M_1]$, and $m_2 \in [-M_2, M_2]$ when $m_1 > 0$, while $m_2 \in [1, M_2]$ when $m_1 = 0$. The set $\bar{M}$ is just the negative of $M$: $\bar{M} = \{(m_1, m_2) : (-m_1, -m_2) \in M\}$. Since $G$ is real, the Fourier coefficients with indices in $\bar{M}$ are related to those with indices in $M$, $g(-m_1, -m_2) = g^*(m_1, m_2)$.

For ease of notation, Fourier series are written using indices in the union of the two sets $M \cup \bar{M}$, even though the corresponding amplitudes are not independent. Written using just the set $M$, the summation in Eqn. (11) becomes $\sum_{\mathbf{m} \in M} 2\,\mathrm{Re}\left[g(\mathbf{m}, J, s) e^{i\mathbf{m}\cdot\mathbf{\Phi}}\right]$; this formula is used in numerical computations.

A projection of the Hamilton-Jacobi equation onto the above Fourier basis gives

$$\partial_s g(\mathbf{m}, \mathbf{J}, s) + i\mathbf{m} \cdot \mathbf{\Omega}(s) g(\mathbf{m}, \mathbf{J}, s) + v(\mathbf{m}, \mathbf{J}, s; g) = 0 \quad , \quad \mathbf{m} \in M \ . \tag{13}$$

Here $v(\mathbf{m}, \mathbf{J}, s; g)$ is the Fourier transform of the perturbation and is a functional of the Fourier coefficients $\{g(\mathbf{m}, \mathbf{J}, s), \mathbf{m} \in M\}$ through the action transformation in Eqn.(8):

$$v(\mathbf{m}, \mathbf{J}, s; g) = \int_0^{2\pi} \frac{d\mathbf{\Phi}}{(2\pi)^d} e^{-i\mathbf{m}\cdot\mathbf{\Phi}} V\Big(\mathbf{\Phi}, \mathbf{J} + G_{\mathbf{\Phi}}(\mathbf{\Phi}, \mathbf{J}, s), s\Big) \quad , \tag{14}$$

$$G_{\mathbf{\Phi}}(\mathbf{\Phi}, \mathbf{J}, s) = \sum_{\mathbf{m} \in M \cup \bar{M}} i\mathbf{m} g(\mathbf{m}, \mathbf{J}, s) e^{i\mathbf{m}\cdot\mathbf{\Phi}} \quad . \tag{15}$$

Recall that the set $M \cup \bar{M}$ does not contain the mode $\mathbf{m} = \mathbf{0}$, so that Eqn. (13) does not involve $\mathbf{m} = \mathbf{0}$, and is independent of the choice of $H_1(\mathbf{J}, s)$. Hence, it can be solved for $g(\mathbf{m}, \mathbf{J}, s)$ with $\mathbf{m} \neq \mathbf{0}$ subject to the $s$-periodicity condition. This completely determines $G_{\mathbf{\Phi}}$ when $\mathbf{J}$ is specified.

Projection of the Hamilton-Jacobi equation onto the $\mathbf{m} = \mathbf{0}$ mode gives

$$H_1(\mathbf{J}, s) = \mathbf{\Omega}(s) \cdot \mathbf{J} + \partial_s g(\mathbf{0}, \mathbf{J}, s) + v(\mathbf{0}, \mathbf{J}, s; g) \quad . \tag{16}$$

Since $v(\mathbf{0}, \mathbf{J}, s; g)$ is determined by $G_{\mathbf{\Phi}}$ alone, and the solution of Eqn. (13) gives $G_{\mathbf{\Phi}}$, we determine $H_1$ by an arbitrary, $s$-periodic choice of $g(\mathbf{0}, \mathbf{J}, s)$.

It is convenient to choose $g(\mathbf{0}, \mathbf{J}, s)$ to be zero. Different choices give different definitions of the new angle $\mathbf{\Psi}$, but the differences are innocuous, in that the change of $\mathbf{\Psi}$ during a period of $s$ is always the same. The perturbed tune, or winding number, $\boldsymbol{\nu}'$ gives the change in $\mathbf{\Psi}$ in one turn normalized by $2\pi$: $\mathbf{\Psi}(C) - \mathbf{\Psi}(0) = 2\pi\boldsymbol{\nu}'$. From Hamilton's equation for the evolution of $\mathbf{\Psi}$, the tune is

$$\boldsymbol{\nu}' = \frac{1}{2\pi} \int_0^C \partial_{\mathbf{J}} H_1(\mathbf{J}, s) ds = \boldsymbol{\nu} + \frac{1}{2\pi} \int_0^C \partial_{\mathbf{J}} v(\mathbf{0}, \mathbf{J}, s; g)\, ds \quad , \tag{17}$$

where $\boldsymbol{\nu}$ is the tune of the unperturbed motion,

$$2\pi\boldsymbol{\nu} = \int_0^C \mathbf{\Omega}(\sigma) d\sigma \quad . \tag{18}$$

Owing to periodicity in $s$, the term $\partial_s g$ in $H_1$ does not contribute to the integral (17) , and the tune is invariant to changes in the choice of $g(\mathbf{0}, \mathbf{J}, s)$.

The linear term in Eqn. (13) can be eliminated by using the integrating factor $\exp\left(i\mathbf{m}\cdot\mathbf{X}(s)\right)$, where

$$\mathbf{X}(s) = \int_0^s \mathbf{\Omega}(\sigma)d\sigma \tag{19}$$

is the linear phase advance, $\mathbf{\Phi}(s) - \mathbf{\Phi}(0)$. Eqn. (13) becomes

$$\partial_s h(\mathbf{m},\mathbf{J},s) = -e^{i\mathbf{m}\cdot\mathbf{X}(s)} v\Big(\mathbf{m},\mathbf{J},s;g(h)\Big)\ , \quad \mathbf{m}\in M\ , \tag{20}$$

where

$$h(\mathbf{m},\mathbf{J},s) = e^{i\mathbf{m}\cdot\mathbf{X}(s)} g(\mathbf{m},\mathbf{J},s) \quad . \tag{21}$$

The periodicity of $g$ in $s$ implies the boundary condition on the new variable $h$:

$$h(\mathbf{m},\mathbf{J},C) = e^{2\pi i\mathbf{m}\cdot\boldsymbol{\nu}} h(\mathbf{m},\mathbf{J},0) \quad . \tag{22}$$

Notice that $h$ has the nice property of being constant over any interval of $s$ in which the perturbation vanishes, *i.e.*, any region in which magnetic fields are linear or zero.

Periodicity of a solution $g(\mathbf{m},\mathbf{J},s)$ of (13) implies periodicity of its derivatives with respect to $s$, at least at generic points where $V$ and $\mathbf{\Omega}$ are sufficiently smooth. Suppose, for instance, that $\mathbf{\Omega}(s)$ and $V(\mathbf{\Phi},\mathbf{J},s)$ are continuous in $s$ in a neighborhood of $s_0$, and that $V$ is continuous as a function of $\mathbf{J}$. Then (13) shows that $\partial_s g(\mathbf{m},\mathbf{J},s)$ is continuous near $s_0$, and periodic in $s$ with period $C$. By differentiating (13), and assuming more smoothness of $V$ and $\mathbf{\Omega}$, one can make similar conclusions about higher derivatives. In the accelerator problem, smoothness will be lacking only at sharp edges of magnets.

The differential relations and boundary conditions for the $h$ coefficients are summarized below:

$$\partial_s h(\mathbf{m},\mathbf{J},s) = -e^{i\mathbf{m}\cdot\mathbf{X}(s)} v\Big(\mathbf{m},\mathbf{J},s;g(h)\Big) \quad , \quad \mathbf{m}\in M \quad , \tag{23}$$

$$v\Big(\mathbf{m},\mathbf{J},s;g(h)\Big) = \int_0^{2\pi} \frac{d\mathbf{\Phi}}{(2\pi)^d} e^{-i\mathbf{m}\cdot\mathbf{\Phi}} V(\mathbf{\Phi},\mathbf{J}+G_{\mathbf{\Phi}},s) \quad , \tag{24}$$

$$G_{\mathbf{\Phi}} = \sum_{\mathbf{m}\in M\cup\bar{M}} i\mathbf{m}h(\mathbf{m},\mathbf{J},s) e^{i\mathbf{m}\cdot\left(\mathbf{\Phi}-\mathbf{X}(s)\right)} \quad , \tag{25}$$

$$h(\mathbf{m},\mathbf{J},C) = e^{2\pi i\mathbf{m}\cdot\boldsymbol{\nu}} h(\mathbf{m},\mathbf{J},0) \quad . \tag{26}$$

In the next section, we describe a method to find solutions of Eqn. (23) consistent with Eqn. (26).

## III. SOLUTION BY THE SHOOTING METHOD

In this section, we discuss the solution of Eqns. (23)–(26) for the Fourier amplitudes $h(\mathbf{m},\mathbf{J},s)$. We formulate the problem as one of finding the fixed point of a nonlinear map. We close this section with a discussion of the numerical methods for evaluating the map and for finding its fixed point.

Eqns. (23)–(25) define the evolution of the initial conditions $h(\mathbf{m},\mathbf{J},s=0)$ to the final values $h(\mathbf{m},\mathbf{J},s=C)$. The integration of Eqn. (23) from an arbitrary initial condition $h(0)$ to a final value $h(C)$ defines the map $U$:

$$h(C) - h(0) = U\big(h(0)\big) \quad . \tag{27}$$

Here and elsewhere we suppress reference to $\mathbf{m}$ and $\mathbf{J}$, and write $h(s)$ for the vector with components $h(\mathbf{m},\mathbf{J},s)$. The boundary condition (26) is not satisfied for an

arbitrary $h(0)$. In terms of the evolution map $U$, the boundary condition demands that $h(0)$ satisfy the equation

$$h(\mathbf{m},\mathbf{J},0) = \frac{1}{e^{2\pi i \mathbf{m}\cdot\boldsymbol{\nu}} - 1} U\big(\mathbf{m},\mathbf{J},h(0)\big) \quad . \tag{28}$$

In other words, we seek a fixed point $h(0)$ of the map $A$ ,

$$h(0) = A(h(0)) \quad , \tag{29}$$

where

$$A\big(\mathbf{m},\mathbf{J},h(0)\big) = \frac{1}{e^{2\pi i \mathbf{m}\cdot\boldsymbol{\nu}} - 1} U\big(\mathbf{m},\mathbf{J},h(0)\big) \tag{30}$$

An essential property of this formulation is that $A$ is proportional to the perturbation strength $V$. This makes it feasible to solve the fixed point problem by iteration, when $V$ is sufficiently small, and the divisor $e^{2\pi i \mathbf{m}\cdot\boldsymbol{\nu}} - 1$ is bounded away from zero by an appropriate choice of the mode set $M$ and the unperturbed tune $\boldsymbol{\nu}$. The change of variable from $g$ to $h$ was needed to create an operator proportional to $V$; the corresponding step in quantum mechanics is to use the interaction picture.

To solve Eqn. (28), we use standard techniques from the study of fixed points of nonlinear maps.[13,14] We describe these methods in detail below.

# A. Simple Iteration

The most obvious method to find the fixed point of Eqn. (28) is referred to here as simple iteration. The iteration proceeds in the following manner, $h^{i+1}(0) = A\big(h^i(0)\big)$, with the superscript $i$ labeling different iterates. A proof of convergence to a unique fixed point is described in Appendix I.

Our initial guess, $h^0(0)$, will be the approximate solution of Eqns. (23)–(26) to lowest order in perturbation theory. This is obtained by putting $G_{\Phi}$ equal to zero in the right hand side of Eqn. (24). Then Eqn. (24) can be evaluated explicitly using Eqns. (2) and (4) . The resulting initial iterate is

$$h^0(\mathbf{m},\mathbf{J},0) = \frac{ie^{-i\pi\mathbf{m}\cdot\boldsymbol{\nu}}}{2\sin\pi\mathbf{m}\cdot\boldsymbol{\nu}} \int_0^C e^{i\mathbf{m}\cdot\mathbf{X}(s)}\, v(\mathbf{m},\mathbf{J},s)\, ds \quad , \tag{31}$$

with

$$\begin{aligned} v(\mathbf{m},\mathbf{J},s) = \frac{\sqrt{2}}{4}\sum_{n=1}^{N} f_n(s)S_n\Big\{ & \delta\big(\mathbf{m}-(3,0)\big)\frac{1}{6}\big(J_1\beta_1(s)\big)^{3/2} \\ & + \delta\big(\mathbf{m}-(1,0)\big)\Big(\frac{1}{2}\big(J_1\beta_1(s)\big)^{3/2} - \big(J_1\beta_1(s)\big)^{1/2}J_2\beta_2(s)\Big) \\ & - \Big(\delta\big(\mathbf{m}-(1,2)\big)+\delta\big(\mathbf{m}-(1,-2)\big)\Big)\frac{1}{2}\big(J_1\beta_1(s)\big)^{1/2}J_2\beta_2(s)\Big\} \end{aligned} \tag{32}$$

with $\mathbf{m} \in M$. The $\delta\big(\mathbf{m}-(j,k)\big)$ are Kronecker deltas with the value 1 when $\mathbf{m} = (j,k)$ and 0 otherwise, and the summation is carried out over $N$ sextupole magnets of strength $S_n$; see Eqn. (4). Notice, at $s = 0$ the $h$ and $g$ coefficients are equal.

The notorious problem of small divisors near resonances can be seen in the leading factor in Eqn. (30). The denominator vanishes when $\mathbf{m}\cdot\boldsymbol{\nu} = p$, where $p$ is an integer. The iterative procedure cannot succeed unless the mode set $M$ and

the unperturbed tune $\boldsymbol{\nu}$ are chosen so that the denominator is nonvanishing. The smaller the minimum value of the denominator, the smaller the perturbation $V$ must be to secure convergence of the iteration. It follows that for a fixed $V$ this method cannot provide arbitrary accuracy. If one attempts to increase accuracy by expanding the set of Fourier modes, the minimum divisor tends to zero, since there are vectors $\boldsymbol{\nu}_r$ with rational components close to any $\boldsymbol{\nu}$ whatever. As we shall see, this deterioration of convergence is clearly observed in computations.

## B. Newton Iteration

To expand the domain of convergence, we turn to Newton's method. The small divisors have the same impact in this method, even though their role is a bit less obvious. Nevertheless, for a given $M$ and $\boldsymbol{\nu}$, the Newton method succeeds for much larger $V$ than can be handled in simple iteration.

The desired fixed point is the solution to the complex-valued vector equation,

$$F\big(h(0)\big) = A\big(h(0)\big) - h(0) = 0 \quad . \tag{33}$$

In Newton's method we make a first-order Taylor expansion of $F$ around a given iterate to define the next iterate as a solution of linear equations.

The derivative of $F$ is not well-defined in the sense of complex function theory: $F$ is not an analytic function of $h(0)$. Eqn. (33) should be written as two real equations, then the derivative of $F$ with respect to $\mathrm{Re}\, h$ and $\mathrm{Im}\, h$ is well-defined. We use a compact notation for the real equations, $\tilde{F} = (\mathrm{Re}\, F, \mathrm{Im}\, F)^T$, and $\tilde{h}(0) = \big(\mathrm{Re}\, h(0), \mathrm{Im}\, h(0)\big)^T$. Then Eqn. (33) takes the form $\tilde{F}\big(\tilde{h}(0)\big) = 0$.

To state equations in components, we write $\tilde{h}(\mathbf{m})$ for $\tilde{h}(\mathbf{m},\mathbf{J},0)$. Then Newton's method is defined by the equations

$$\tilde{F}(\mathbf{m},\tilde{h}^i) + \sum_{\mathbf{n}\in M} \tilde{D}(\mathbf{m},\mathbf{n},\tilde{h}^i)\cdot[\tilde{h}^{i+1}(\mathbf{n}) - \tilde{h}^i(\mathbf{n})] = 0 \quad , \tag{34}$$

with

$$\tilde{D}(\mathbf{m},\mathbf{n},\tilde{h}) = \begin{pmatrix} \partial \operatorname{Re} F(\mathbf{m},\tilde{h})/\partial \operatorname{Re} h(\mathbf{n}) & \partial \operatorname{Re} F(\mathbf{m},\tilde{h})/\partial \operatorname{Im} h(\mathbf{n}) \\ \partial \operatorname{Im} F(\mathbf{m},\tilde{h})/\partial \operatorname{Re} h(\mathbf{n}) & \partial \operatorname{Im} F(\mathbf{m},\tilde{h})/\partial \operatorname{Im} h(\mathbf{n}) \end{pmatrix} . \tag{35}$$

This system of equations is solved for the new iterate $\tilde{h}^{i+1}$, given $\tilde{h}^i$, by a direct method (Gaussian elimination). The Jacobian $\tilde{D}$ of the map is approximated numerically by divided differences. Each component of $\tilde{h}$ is perturbed separately by a small amount, and $\tilde{F}$ computed at perturbed and unperturbed points. The matrix elements of the Jacobian are then found as

$$\begin{aligned} \frac{\partial F(\mathbf{m},\tilde{h})}{\partial \operatorname{Re} h(\mathbf{n})} &= \frac{F(\mathbf{m},h+(e(\mathbf{n}),0)^T\delta h) - F(\mathbf{m},h)}{\delta h} \quad , \\ \frac{\partial F(\mathbf{m},\tilde{h})}{\partial \operatorname{Im} h(\mathbf{n})} &= \frac{F(\mathbf{m},h+(0,ie(\mathbf{n}))^T\delta h) - F(\mathbf{m},h)}{\delta h} \quad , \end{aligned} \tag{36}$$

where $\delta h$ is a small real number and $e(\mathbf{n}) = \{\delta(\mathbf{p}-\mathbf{n}), \mathbf{p}\in M\}$ is the unit vector in the direction corresponding to mode $\mathbf{n}$. In practice, we take $\delta h = (10^{-6} - 10^{-5})|h(\mathbf{n})|$.

The larger domain of convergence of Newton's method is achieved at a computational expense that becomes significant for $d \geq 2$. The expense is mainly due to the Jacobian evaluation. With $d = 2$ the total number of independent modes in the set $M$ is $2M_1M_2 + M_1 + M_2$. In a typical calculation we might have $M_1 = M_2 = 15$, hence 480 independent modes and 960 map evaluations to

approximate the Jacobian. For a general $d$-dimensional mode vector the number of independent components is a little more than $2^{d-1}M_1M_2\ldots M_d$. The calculation of the Jacobian quickly becomes untenable as the mode set or the number of degrees of freedom is increased. In contrast, the simple iteration requires only one evaluation of the map $A(h)$ at each iteration.

We employ two methods to reduce the time for the Jacobian calculation. First, Broyden's update method is used to approximate the Jacobian. Second, we discard many modes within the mode set $M$.

## C. Newton-Broyden Iteration

For the Newton-Broyden iteration, the Jacobian of the map is calculated fully only once and is afterward updated using the Broyden algorithm.[15–17] If $\tilde{D}^i$ is the Jacobian at the $i$-th iteration then the update of the Jacobian at the $(i+1)$-th iteration is

$$\tilde{D}^{i+1} = \tilde{D}^i + \frac{[\tilde{F}(\tilde{h}^{i+1}) - \tilde{F}(\tilde{h}^i) - \tilde{D}^i\,(\tilde{h}^{i+1} - \tilde{h}^i)] \cdot (\tilde{h}^{i+1} - \tilde{h}^i)^T}{(\tilde{h}^{i+1} - \tilde{h}^i)^T \cdot (\tilde{h}^{i+1} - \tilde{h}^i)} \quad . \tag{37}$$

The $\tilde{h}$ are treated as column vectors, and the $\tilde{h}^T$ as corresponding row vectors. The costly computation (36) is used only to find $\tilde{D}^0$; each subsequent iteration requires only one new map evaluation, $\tilde{F}(\tilde{h}^{i+1})$.

The domain of convergence of the Newton-Broyden iteration is still large while computation times are much more reasonable than those of a full Newton iteration. In practice it converges for strong effective nonlinearities, in particular, for initial conditions close to the dynamic aperture in accelerator problems.

A more daring and still more economical approximation can be attempted. If $A$ were zero in Eqn. (33), the Jacobian would be $-\mathbf{1}$. Putting $\tilde{D}^0 = -\mathbf{1}$ in (37), we were surprised to find that the Broyden updates still provided a region of convergence substantially larger than that of simple iteration. In comparison to the calculation with $\tilde{D}^0$ from divided differences, the region of convergence was somewhat smaller, and more iterations were required for adequate convergence.

## D. Mode Selection

To achieve a certain accuracy, one has to choose a minimum value for the maximum mode numbers $M_i$. On the other hand, for a given choice of $M_i$ there are usually many amplitudes of modes with $|m_i| < M_i$ that are quite negligible. We apply a simple technique to identify and eliminate the negligible modes within the set $M$.

We carry out one simple iteration using the full mode set $M$, as in Section A above. We then compute the evolution in $s$ of the resulting $h(0)$, and for each $\mathbf{m}$ the maximum over $s$ of $|h(\mathbf{m}, \mathbf{J}, s)|$. When the latter is less than some fixed small fraction of $\max_{\mathbf{n}} \max_s |h(\mathbf{n}, \mathbf{J}, s)|$, we throw away mode $\mathbf{m}$ in all subsequent computations. In our examples with $d = 2$, no more than 130 to 200 complex amplitudes are retained. Since the time to approximate the initial Jacobian goes down with the square of the number of amplitudes, a great deal of time is saved.

## E. Numerical Integration

The nonlinear map $U$ of Eqn. (28) must be evaluated by numerical integration of Eqn. (23). We use a fourth order Runge-Kutta algorithm. Recall that $h(\mathbf{m}, \mathbf{J}, s)$ changes only over the support of the nonlinear perturbation $V$. Thus, in our example the numerical integration need be performed only over the extent of the sextupole magnets. The final value $h(\mathbf{m}, \mathbf{J}, C)$ obtained by the integration is used in Eqn. (27) to calculate the map $U$. After the iteration converges to the fixed point $h(\mathbf{m}, \mathbf{J}, 0)$, the coefficients can be evolved in $s$ using the same fourth order Runge-Kutta algorithm.

It has been observed that the number of Runge-Kutta integration steps per nonlinear element must be increased to maintain accuracy as the effective nonlinearity is increased by going to large amplitudes $\mathbf{J}$. Similarly, the number of $\mathbf{\Phi}$ modes must increase. The number of integration steps in the $s$-direction along the $(d+1)$-dimensional torus is analogous to the number of Fourier modes to represent variation along the $\mathbf{\Phi}$ direction. As the nonlinearity increases, the invariant torus becomes more distorted in both the $s$ and the $\mathbf{\Phi}$ directions, so that both the number of steps and the number of modes must go up.

Working at large amplitudes and using the above stated guess for $h^0$, we find that the iteration can reach a fixed point only for a relatively small number of integration steps. To perform the calculation at a large number, the result from an intermediate number of steps must be used as the starting point. The fixed point found at the intermediate point is then used as the initial iterate for a calculation with a larger number of integration steps. This has the added advantage of cal-

culating the initial Jacobian with a smaller number of integration steps and thus saving computing time.

# IV. TESTS OF THE METHOD

We test the technique introduced in the previous section on two model problems that can be solved analytically. For the case of two autonomous, linearly coupled harmonic oscillators, we compare the exact invariant surface with that from numerical solution of the Hamilton-Jacobi equation. We also compare the analytic and numerical tune shifts for a linear example in which uncoupled betatron motion is perturbed by a quadrupole term.

## A. Linearly coupled harmonic oscillators

For two linearly coupled harmonic oscillators, the Hamiltonian can be written as

$$H(\mathbf{x}, \mathbf{p}_x) = \frac{1}{2}{\mathbf{p}_x}^T \cdot \mathbf{p}_x + \frac{1}{2}\mathbf{x}^T \cdot K_c \cdot \mathbf{x} \quad ,$$
$$K_c = \begin{pmatrix} 1/\beta_1^2 & \Gamma \\ \Gamma & 1/\beta_2^2 \end{pmatrix} \quad . \tag{38}$$

Now the $\beta_i$ are constants, but they are defined in analogy to the $\beta_i(s)$ of Eqn. (1). The $\mathbf{x}$ and $\mathbf{p}_x$ are column vectors of coordinates $(x_1, x_2)^T$ and momenta $(p_1, p_2)^T$, respectively. Since Eqn. (38) is independent of $s$ there exists a canonical transformation producing an uncoupled Hamiltonian. This is equivalent to a transformation diagonalizing the matrix $K_c$.

For the numerical solution of the Hamilton-Jacobi equation, the coupling term $\Gamma x_1 x_2$ serves as the perturbation. Written in the action-angle variables of the

unperturbed Hamiltonian, the full Hamiltonian has the form

$$H(\mathbf{\Phi},\mathbf{I}) = \mathbf{\Omega}_0 \cdot \mathbf{I} + 2\Gamma\sqrt{\beta_1\beta_2 I_1 I_2}\cos\Phi_1\cos\Phi_2 \quad , \tag{39}$$

where $\mathbf{\Omega}_0 = (1/\beta_1, 1/\beta_2)$ and $x_i = \sqrt{2\beta_i I_i}\cos\Phi_i, \quad p_i = -\sqrt{2I_i/\beta_i}\sin\Phi_i$.

Let $(\mathbf{u}, \mathbf{p}_u)$ be variables in which the Hamiltonian appears uncoupled. They are related to the original variables $(\mathbf{x}, \mathbf{p}_x)$ by the orthogonal transformation $S$ that diagonalizes $K_c$; we let $K_d = S^T K_c S$, where $K_d = \mathrm{diag}(1/\beta_{1u}^2, 1/\beta_{2u}^2)$. The new beta parameters $\beta_{iu}$ for the uncoupled case are related to the eigenvalues of the matrix $K_c$ through the above definition of $K_d$. The matrix $S$ is

$$S = |N|\begin{pmatrix} A & -\Gamma \\ \Gamma & A \end{pmatrix} \quad , \tag{40}$$

where

$$\begin{aligned} |N|^{-2} &= 2\left[\Delta^2 + \Gamma^2 + \Delta\sqrt{\Delta^2+\Gamma^2}\right] \quad , \\ A &= \Delta + \sqrt{\Delta^2+\Gamma^2} \quad , \\ \Delta &= \frac{1}{2}\left(\frac{1}{\beta_1^2} - \frac{1}{\beta_2^2}\right) \quad , \end{aligned} \tag{41}$$

The beta parameters for the $\mathbf{u}$-motion found from the eigenvalues of $K_c$ are

$$\begin{pmatrix} 1/\beta_{1u}^2 \\ 1/\beta_{2u}^2 \end{pmatrix} = \begin{pmatrix} \Sigma + \sqrt{\Delta^2+\Gamma^2} \\ \Sigma - \sqrt{\Delta^2+\Gamma^2} \end{pmatrix} \quad , \tag{42}$$

with

$$\Sigma = \frac{1}{2}\left(\frac{1}{\beta_1^2} + \frac{1}{\beta_2^2}\right) \quad .$$

The parameters are chosen so that the right hand side of Eqn. (42) is positive. The $\beta_{iu}$ are defined to be positive.

We take the following steps to generate points on an invariant surface $\mathbf{I}(\mathbf{\Phi})$ to compare with the numerical solution of the Hamilton-Jacobi equation. We introduce the action-angle variables $(\mathbf{I}_u, \mathbf{\Phi}_u)$ of the uncoupled motion. To generate points on the torus, we hold $\mathbf{I}_u$ fixed and allow $\mathbf{\Phi}_u$ to vary on a uniform 40 by 40 grid. Working through the transformations

$$(\mathbf{\Phi}_u, \mathbf{I}_u) \mapsto (\mathbf{u}, \mathbf{p}_u) \mapsto (\mathbf{x}, \mathbf{p}_x) \mapsto (\mathbf{\Phi}, \mathbf{I}) \quad , \tag{43}$$

we finally obtain points $\mathbf{I}(\mathbf{\Phi})$ with invariant action $\mathbf{I}_u$ to compare with the numerical solution of the Hamilton-Jacobi equation. The action-angle transformation is

$$I_i = \frac{1}{2}\Big(\frac{x_i^2}{\beta_i} + \beta_i p_i^2\Big) \quad , \quad \tan\Phi_i = -\beta_i \frac{p_i}{x_i} \quad , \quad i = 1,2 \quad . \tag{44}$$

As a measure of the difference between the Hamilton-Jacobi solution $\mathbf{I}^{HJ}$ and the analytic solution $\mathbf{I}^A$, we compute the normalized sum of deviations

$$\delta_i = \frac{\sum_{\mathbf{\Phi}_u} |I_i^{HJ}\Big(\mathbf{\Phi}(\mathbf{\Phi}_u)\Big) - I_i^A\Big(\mathbf{\Phi}(\mathbf{\Phi}_u)\Big)|}{\sum_{\mathbf{\Phi}_u} |I_i^{HJ}\Big(\mathbf{\Phi}(\mathbf{\Phi}_u)\Big) - I_{ui}|} \quad , \quad i = 1,2 \quad . \tag{45}$$

The summation is over the 40 by 40 grid in the $\mathbf{\Phi}_u$ space.

TABLE I gives the values of $\delta_i$ found for several coupling strengths $\Gamma$ with $\mathbf{I}_u =$ ($10^{-5}$ m, $10^{-5}$ m), $\beta_1 = .50336$ m, $\beta_2 = 1.29322$ m, and a ring circumference of 1 m. The mode spectrum was truncated to $M_1 = M_2 = 7$, giving 112 independent complex modes. A subset of significant modes within this set was selected by the method described in the previous section. The analytic and Hamilton-Jacobi

TABLE I. Comparison of surfaces from the Hamilton-Jacobi equation with analytic surfaces for the linear coupling model with different coupling strengths $\Gamma$. The parameters $\delta_i$, defined as in Eqn.(45), measure the discrepancy.

| $C = 1.0\text{m}, \quad \mathbf{I}_u = 10^{-5}\text{m}, \quad M_1 = M_2 = 7$ | | | |
|---|---|---|---|
| $\Gamma$ ($\text{m}^{-2}$) | $\delta_1$ | $\delta_2$ | modes selected |
| 0.04 | $1.406 \cdot 10^{-4}$ | $2.881 \cdot 10^{-4}$ | 5 |
| 0.10 | $5.799 \cdot 10^{-4}$ | $6.606 \cdot 10^{-4}$ | 7 |
| 0.50 | $5.430 \cdot 10^{-5}$ | $6.186 \cdot 10^{-5}$ | 42 |
| 0.65 | $3.782 \cdot 10^{-4}$ | $11.480 \cdot 10^{-4}$ | 38 |

invariant solutions agree very well. Notice that at $\Gamma = 0.50$ $\text{m}^{-2}$ more modes are kept and a significant increase in accuracy over the other cases is achieved.

FIGs. 1 and 2 show the two components of the invariant surface, normalized by $I_{1u}$ and $I_{2u}$, at any s (time-independent problem) and for $\Gamma = 0.65$ $\text{m}^{-2}$. They are displayed as functions of the angles $\mathbf{\Phi}$, normalized by $2\pi$, and on a vertical scale with 0 at the origin. In terms of the generating function, we are plotting $I_i/I_{iu} = 1 + G_{\Phi_i}(\mathbf{\Phi}, \mathbf{I}_u)/I_{iu}$, with $i = 1, 2$. The constants $\mathbf{I}_u$ serve to distinguish different surfaces. Notice that the departure from a plane surface is quite pronounced. In FIG. 1 showing the $I_1$ surface, the distortion is $\pm 61\%$, and in FIG. 2 showing the $I_2$ surface, it is $\pm 55\%$. This nonlinearity displayed by the coupled variables $I_i$ is of course not an essential feature of this basically linear problem. In problems with genuine nonlinearity one must be careful to separate any effects of linear coupling, which can be confused with the real effects of interest in plots like those of Figures 1 and 2.

## B. Quadrupole perturbation

For a quadrupole perturbation, it is interesting to compare the tune shift found by matrix methods with that from the numerical solution of the Hamilton-Jacobi equation. The perturbation due to a quadrupole is $V = K(s)(x^2 - y^2)/2$, where $K(s)$ is constant within the magnet and zero elsewhere. In action-angle variables, it takes the form $V = K(s)(\beta_1 I_1 \cos^2 \Phi_1 - \beta_2 I_2 \cos^2 \Phi_2)$. The strength $K$ is measured in units of $\mathrm{m}^{-2}$.

From Eqns. (16) and (17) we see that the tune shift in the Hamilton-Jacobi formalism is

$$\boldsymbol{\nu}' - \boldsymbol{\nu} = \frac{1}{2\pi} \frac{\partial}{\partial \mathbf{J}} \int_0^C ds \int_0^{2\pi} \frac{d\boldsymbol{\Phi}}{(2\pi)^N} V\Big(\boldsymbol{\Phi}, \mathbf{J} + G_{\boldsymbol{\Phi}}(\boldsymbol{\Phi}, \mathbf{J}, s), s\Big) \quad . \tag{46}$$

Given $G_{\boldsymbol{\Phi}}$, the integral is calculated with a Simpson's rule for the $s$ integration and with a fast Fourier transform for the $\boldsymbol{\Phi}$ integration. The derivative is estimated with a simple divided difference.

According to lowest order perturbation theory, the tune shift for a weak quadrupole magnet with strength $K$ is

$$\Delta\boldsymbol{\nu} = \frac{1}{4\pi} \int_0^C ds\ K(s) \begin{pmatrix} \beta_x \\ -\beta_y \end{pmatrix} \quad . \tag{47}$$

This can be found using Eqn. (46) and setting $G_{\boldsymbol{\Phi}}$ to zero.

An exact analytic result for the tune shift can be found using matrix methods. Consider two magnetic lattices, one where the first element is a drift (i.e., it corresponds to free particle motion) and another where the drift is replaced by the

quadrupole perturbation. The $4 \times 4$ matrix representations of the full-turn maps of the two lattices can be compared, and the tunes extracted using the traces of the matrices. If the full-turn map for the lattice that begins with the drift element is $T$, then the full-turn map for the same ring, but with the drift replaced by the quadrupole perturbation, is $T' = T \cdot T_D^{-1} \cdot T_Q$, where $T_D$ is the matrix representation for the drift and $T_Q$ is the matrix representation for the quadrupole perturbation:

$$T_D = \begin{pmatrix} 1 & d & 0 & 0 \\ 0 & 1 & 0 & 0 \\ 0 & 0 & 1 & d \\ 0 & 0 & 0 & 1 \end{pmatrix}$$

$$T_Q = \begin{pmatrix} \cos\sqrt{K}\,d & \frac{1}{\sqrt{K}}\sin\sqrt{K}\,d & 0 & 0 \\ -\sqrt{K}\sin\sqrt{K}\,d & \cos\sqrt{K}\,d & 0 & 0 \\ 0 & 0 & \cosh\sqrt{K}\,d & \frac{1}{\sqrt{K}}\sinh\sqrt{K}\,d \\ 0 & 0 & \sqrt{K}\sinh\sqrt{K}\,d & \cosh\sqrt{K}\,d \end{pmatrix} \tag{48}$$

These matrices act on the phase space vector $(x_1, p_1, x_2, p_2)^T$. The length of the drift, and the quadrupole, is $d$ and the quadrupole strength is $K$.

If there is no coupling between $x_1$ and $x_2$ motions, the matrices $T$ and $T'$ are block diagonal; we label the blocks as $T^{(i)}$, $i = 1, 2$. The perturbed tune $\nu_i'$ is obtained from the trace of $T'^{(i)}$ through the formula $2\cos 2\pi\nu_i' = \mathrm{Tr}\, T'^{(i)}$.[18] The matrix $T^{(i)}$ is represented in a standard notation as[18]

$$T^{(i)} = \begin{pmatrix} \cos 2\pi\nu_i + \alpha_i \sin 2\pi\nu_i & \beta_i \sin 2\pi\nu_i \\ -(1+\alpha_i^2)\sin 2\pi\nu_i/\beta_i & \cos 2\pi\nu_i - \alpha_i \sin 2\pi\nu_i \end{pmatrix} \quad , \tag{49}$$

again with $2\alpha_i = -d\beta_i/ds$. The analytic forms for the tune shifts are found to be

$$\cos 2\pi\nu_1' = \cos\sqrt{K}\,d\left(\cos 2\pi\nu_1 + d\,\frac{(1+\alpha_1^2)}{2\beta_1}\sin 2\pi\nu_1\right)$$

$$+\frac{1}{2}\sin\sqrt{K}\,d\left(\sqrt{K}\,d\cos 2\pi\nu_1+(\sqrt{K}\,d\,\alpha_1-\sqrt{K}\beta_1-\frac{(1+\alpha_1^2)}{\sqrt{K}\,\beta_1})\sin 2\pi\nu_1\right) \quad ,$$

$$\cos 2\pi\nu_2' = \cosh\sqrt{K}\,d\left(\cos 2\pi\nu_2+d\,\frac{(1+\alpha_2^2)}{2\beta_2}\sin 2\pi\nu_2\right)$$

$$+\frac{1}{2}\sinh\sqrt{K}\,d\left(-\sqrt{K}\,d\cos 2\pi\nu_2-(\sqrt{K}\,d\,\alpha_2-\sqrt{K}\beta_2+\frac{(1+\alpha_2^2)}{\sqrt{K}\,\beta_2})\sin 2\pi\nu_2\right) . \tag{50}$$

The lattice functions $\alpha_i(s), \beta_i(s)$ are evaluated at the beginning of the drift.

We studied several cases with a single quadrupole of strength varying from $10^{-5}$ to 0.3 $\mathrm{m}^{-2}$. The lattice used for $T$ is that given in the next section in TABLE II with the sextupoles removed, *i.e.*, replaced by drifts. The first sextupole space is either the drift or the quadrupole perturbation in the above discussion. The values of the tune shift from the Hamilton-Jacobi solution, normalized by the quadrupole strength, are compared with the analytic formula given above. The results are in FIGs. 3 and 4. The dotted line follows the analytic formula, Eqn. (50), and the (×) marks results from the numerical solution of the Hamilton-Jacobi equation. The relative error of the Hamilton-Jacobi result, defined as $[\sum(w^{HJ}-w^M)^2/\sum(w^{HJ})^2]^{1/2}$, is $9.97\cdot 10^{-6}$ for $\Delta\nu_1/K$, and $9.73\cdot 10^{-6}$ for $\Delta\nu_2/K$. The sum runs over the points marked by (×), and $w^{HJ}=\Delta\nu_i^{HJ}/K$ is the normalized tune shift from the Hamilton-Jacobi equation, and $w^M=\Delta\nu_i^M/K$ is the analytic result from the matrix method.

The distortion of the invariant surfaces for the largest quadrupole strength of $K = 0.30$ $\mathrm{m}^{-2}$ is ±5.9% for the $I_1$ surface and ±36% for the $I_2$ surface. The constant actions chosen for the above study are $\mathbf{J} = 10^{-5}$m. The results for the tune shift seem to be independent of $\mathbf{J}$ for several different values that were checked.

# V. A NON-INTEGRABLE EXAMPLE: SEXTUPOLES IN A STORAGE RING

We present some examples of numerical solutions of the Hamilton-Jacobi equation in non-integrable cases with $d = 1$ and $d = 2$, with Hamiltonian periodic in the time-like independent variable $s$. The examples are based on a simplified model of an electron storage ring, with the nonlinearity provided by strong sextupole magnets. The behavior of this system is generic, in broad characteristics, for storage ring models with $d \leq 2$, even for models with more elaborate and realistic representations of the magnetic lattice. Indeed, the behavior is fairly generic for a large class of nonlinear systems in various fields of physics.

The sextupole magnets, always present in a modern synchrotron or storage ring, serve to correct the energy dependence of the focusing from the quadrupole magnets. They are placed in a dispersive region of the ring, where particles of different energy have different transverse positions. Since a sextupole field gradient is proportional to the transverse displacement, and since the latter is proportional to the energy deviation, a sextupole can be used to counteract the effect of weaker quadrupole focusing for particles of higher energy. This is called chromatic correction of the focusing.

In addition to the desired chromatic correction, the sextupoles cause undesired nonlinear effects, even though they are arranged with appropriate spacing and strengths so that nonlinear effects cancel to a large extent. At sufficiently large amplitudes of transverse oscillations, the residual nonlinear effects dominate, and lead to unstable motion in which particles are lost from the beam.

The example considered here is a single "cell" of the magnetic lattice for the Berkeley Advanced Light Source (ALS), an electron storage ring operated as a synchrotron radiation source. The cell contains four sextupole magnets. The actual lattice of the ALS contains twelve such cells, now somewhat modified from the early design that we use, and complications from other magnetic elements and errors, all of which we ignore. Our cell is taken from the Berkeley Advanced Light Source Conceptual Design Report.[19] TABLE II gives the relevant parameters describing the cell, in both linear and nonlinear aspects. The position (leading edge), strength, and length of each sextupole magnet is listed, together with the linear lattice parameters $\beta_i(s), \alpha_i(s), X_i(s)$ evaluated with $s$ at the leading edge of the sextupole. The phase advance $X_i$ is defined in Eqn. (19). The linear tunes $\nu_i$, the ring circumference (cell length) $C$, and the initial values of $\beta_i$ and $\alpha_i$ are also listed.

TABLE II. Parameters for a single cell of the ALS storage ring. The first four columns specify the sextupole magnets, while the remaining columns give the linear lattice functions, evaluated at the leading edge of the sextupole.

| C=16.4m, 1/12 of ring, $\nu_1$=1.18973, $\nu_2$=0.68158 | | | | | | | | | |
|---|---|---|---|---|---|---|---|---|---|
| name | position | strength | length | parameters | | | | phase | |
| | m | $m^{-3}$ | m | $\beta_1$, m | $\beta_2$, m | $\alpha_1$ | $\alpha_2$ | $X_1, rads$ | $X_2, rads$ |
| SD | 5.775 | -88.090 | .20 | 1.472 | 10.696 | -1.779 | 8.401 | 2.480 | 0.866 |
| SF | 6.875 | 115.615 | .20 | 3.984 | 1.580 | 2.272 | 0.417 | 2.819 | 1.222 |
| SF | 9.325 | 115.615 | .20 | 3.137 | 1.443 | -1.963 | -0.268 | 4.600 | 2.928 |
| SD | 10.425 | -88.090 | .20 | 2.297 | 7.603 | 2.345 | -7.062 | 4.886 | 3.395 |
| at s=0, $\beta_1$=11 m, $\beta_2$=4 m, $\alpha_1=\alpha_2$=0 | | | | | | | | | |

To gain a broad understanding of single particle motion for this Hamiltonian, a stability plot is made giving initial conditions for trajectories stable or unstable within 5000 turns. Each point in FIG. 5 represents the action **I** of the initial condition for a trajectory. The initial angles $\mathbf{\Phi}$ are zero. The equations of motion are integrated over the nonlinear elements by means of an explicit, fourth order, symplectic integrator.[20] On each turn the trajectory is tested; if the position $x_i$ is greater then 1 m, or the angle $dx_i/ds$ is greater than 1 radian, that trajectory is considered lost or unstable. The stars and dots represent initial conditions of trajectories that are lost or not lost , respectively, after 5000 turns. The boundary between the regions occupied by stars and dots is called the "5000 turn dynamic aperture". More loosely, the "short-term dynamic aperture" usually refers to a few thousand turns. The "physical aperture", imposed by the dimensions of the vacuum chamber in which the particles move, is preferably smaller than the short-term dynamic aperture.

## A. One-Dimensional Example

We first treat one-dimensional motion—only the coordinate $x_1$ is allowed to vary. The trajectories should be stable, under the definition of FIG. 5, out to an initial action around $I_1(\Phi_1 = 0, s = 0) \approx 2 \cdot 10^{-5}$ m. The corresponding maximum value of the constant action $J_1$ will have roughly the same order of magnitude. This yields an approximate upper limit on the constant action that could yield approximate invariant tori from the numerical solution of the Hamilton-Jacobi equation.

In FIG. 6, three representative solutions (approximate invariant tori) with

different constant actions are plotted. These curves are sections of the 2-torus $I_1 = J_1 + G_{\Phi_1}(\Phi_1, J_1, s)$ at $s = 0$ and are plotted as a function of $\Phi_1/2\pi$. The $s$-dependence can be found by evolving the Fourier coefficients with the nonlinear time evolution map as defined in Section III. Several items characterizing each solution of the Hamilton-Jacobi equation are given in Table III.

In TABLE III, the accuracy of the solution $\delta_1$ is estimated by comparing the curve with the result of accurate numerical integration of Hamilton's equations ("tracking"), again using an explicit fourth-order symplectic integrator.[20] Sixteen initial conditions are chosen on the invariant surface, and each is tracked for 1000 turns, thus defining a trajectory. To compare the values of action on the trajectory, $I^{TR}(s = nC)$, with the corresponding values on the computed surface, $I^{HJ}\big(\Phi_1^{TR}(s = nC)\big)$, we define an error parameter

$$\delta_1 = \max_{\{\Phi_{10}\}} \frac{\sum_{n=1}^{1000} |I_1^{HJ}\big(\Phi_1{}^{TR}(s = nC)\big) - I_1^{TR}(s = nC)|}{\sum_{n=1}^{1000} |I_1^{HJ}\big(\Phi_1^{TR}(s = nC)\big) - J_1|} \quad . \tag{51}$$

The summation is over the number of turns the trajectory was followed (1000 turns in this case), and the maximum is taken over a set of 16 initial angles which are uniformly distributed. Notice that $\delta_1$ is normalized so that it measures the error in the departure from linear motion. Instead, one could normalize by replacing the denominator in (51) by $J_1$, so as to measure the error in $I_1$ itself; this would give considerably smaller values.

Several other parameters are given in TABLE III. The distortion of the invariant surface from a plane gives a measure of the strength of the nonlinearity; a similar quantity is called "smear" in accelerator physics.[21] We define the distortion to be the average of the maximum excursion above the mean and the maximum

excursion below the mean, divided by the mean, $J_1$. A characteristic displacement of the trajectory is the value of $x_1$ at $\Phi_1 = 0, s = 0$: $x_{10} = \sqrt{2\beta_1(0)I_1(0)}$. The nonlinear tune shift as defined in the previous section, and the CPU time to find the fixed point on the IBM 3090 Model 200 E, are also shown.

TABLE III. Parameters for numerical solutions of the Hamilton-Jacobi equation with $d = 1$. The corresponding approximate invariant curves are given in FIG. 6.

| case | constant action $J_1$(m) | mode set $M_1$ | tracking comparison $\delta_1$ | initial offset $x_{10}$(mm) | distortion % | tune shift $\Delta\nu$ | cpu time IBM 3090 (s) |
|---|---|---|---|---|---|---|---|
| a | $2 \cdot 10^{-7}$ | 15 | $1.51 \cdot 10^{-5}$ | 2.1 | $\pm 2.8$ | $-1.068 \cdot 10^{-4}$ | 5 |
| b | $2 \cdot 10^{-6}$ | 31 | $1.04 \cdot 10^{-4}$ | 7.5 | $\pm 9.0$ | $-1.073 \cdot 10^{-3}$ | 19 |
| c | $2 \cdot 10^{-5}$ | 63 | $3.67 \cdot 10^{-3}$ | 21.4 | $\pm 31.6$ | $-1.220 \cdot 10^{-2}$ | 28 |

As the amplitude $J_1$ increases, a larger mode set (all modes in the set are being selected) is required to maintain even moderate accuracy. The tune shift is approximately linear with amplitude, as is expected for sextupole magnets. The initial offset $x_{10}$ for case (c) comes close to the value 22.5 mm given in the ALS Conceptual Design Report[19] for the maximum $x_1$ coordinate of the short-term dynamic aperture of the ideal lattice (i.e., the configuration of magnets that we study, without errors).

## B. Two-Dimensional Example

We present several results for the full two-dimensional sextupole problem. We discuss the tune shifts found from a family of approximate solutions and show that they are almost linear in the constant actions. We also present two solutions in detail: one for small **J** and one for large **J**.

In FIGs. 7 and 8, the nonlinear tune shifts, found from several numerical solutions, are plotted in a contour plot as functions of the constant actions $J_1$ and $J_2$. The $(\times)$ marks points where numerical solutions of the Hamilton-Jacobi equation were found. The tune shifts were fitted to a global, cubic polynomial in the constant actions, and this was used to make the contour plots. The discrepancy between the fit and the data, measured by the root mean square of the deviation normalized by the data, was $2.61 \cdot 10^{-3}$ for $\Delta\nu_1$ and $2.27 \cdot 10^{-3}$ for $\Delta\nu_2$. From the figures and the fit, it is clear that the tune shifts are nearly linear functions of the actions. This is what is expected for sextupole nonlinearities from low order perturbation theory.

The solutions found for FIGs. 7 and 8 used the modest mode set of $M_1 = M_2 = 7$. Of the 112 modes only the 30 largest were selected to do the calculation. This kept the computation time for the solution at the largest value of the action $\mathbf{J} = (6 \cdot 10^{-6}\mathrm{m}, 6 \cdot 10^{-6}\mathrm{m})$ to 271 seconds on the IBM 3090. Comparison with short term tracking, as described above, gives $\delta_1 \leq 0.31$ and $\delta_2 \leq 0.56$, and these large values only for the largest **J**. The majority of the solutions in the figures give $\delta_i \leq 10^{-2}$. The two-dimensional $\delta_i$ are defined in analogy to the one-dimensional case. In the two-dimensional definition, the initial angles $(\Phi_{10}, \Phi_{20})$ are distributed

evenly in a 4 by 4 grid in the $\mathbf{\Phi}$ plane.

In FIGs. 9–12, we give three-dimensional plots of invariant surfaces, showing $I_1(\mathbf{\Phi},\mathbf{J},0)/J_1$ and $I_2(\mathbf{\Phi},\mathbf{J},0)/J_2$ as functions of $(\Phi_1/2\pi,\Phi_2/2\pi)$ for $J_1 = J_2 = 2\cdot 10^{-7}$ m and $J_1 = J_2 = 4\cdot 10^{-6}$ m, respectively. As expected, the distortion from a planar surface is greater for the case with larger constant action. In the initial action space of FIG. 5, these two solutions correspond to points A and B.

TABLE IV gives some relevant parameters for the two-dimensional solutions shown in FIGs. 9–12, as well as two other solutions, indicated as C and D, whose invariant surfaces we do not show. The corresponding initial actions for C and D are given in FIG. 5. All solutions have $M_1 = M_2$. The number of modes actually used in the calculation is shown, along with the total number of independent modes in the set from which they were selected. The initial number and final number of integration steps per sextupole are given under $N_{RK}$ (number of full Runge-Kutta steps, each requiring four evaluations of the right-hand side of the differential equation). The parameters giving the comparison to short term tracking are shown as $\delta_i$. The distortion from a planar surface is reported for each case; it is defined as the average of the excursions above and below unity of the ratio $I_i/J_i$. Finally we give the total computation time, including both the surface calculation and program diagnostics, on the SLAC IBM 3090 Model 200 E ; the time is dominated by the surface calculation.

We see from TABLE IV that for larger actions, and greater distortions, a larger mode set must be used and more modes must be chosen to represent the surface accurately. Larger actions also require more integration steps per nonlinear element to get numerical convergence to a fixed point. This leads to a big increase in the

TABLE IV. Parameters for representative numerical solutions in two-dimensions including those in FIGs. 9–12. These correspond to the initial conditions marked in FIG. 5.

| case | $J_1$,$J_2$ ($10^{-6}$m) | set $M_i$ | modes | $N_{RK}$ | tracking $\delta_1$ | tracking $\delta_2$ | distortion (%) $I_1$ | distortion (%) $I_2$ | cpu time IBM 3090 |
|---|---|---|---|---|---|---|---|---|---|
| A | 0.2, 0.2 | 15 | 50/480 | 2/10 | $2.66 \cdot 10^{-4}$ | $4.37 \cdot 10^{-4}$ | ±6.2 | ±4.6 | 14m57s |
| B | 4, 4 | 31 | 180/1984 | 7/16 | $3.88 \cdot 10^{-2}$ | $1.62 \cdot 10^{-2}$ | ±33.3 | ±27.9 | 3h13m10s |
| C | 1, 3 | 31 | 125/480 | 5/16 | $5.64 \cdot 10^{-3}$ | $5.16 \cdot 10^{-3}$ | ±35.4 | ±12.2 | 1h37m28s |
| D | 3, 1 | 31 | 180/1984 | 4/16 | $5.73 \cdot 10^{-4}$ | $9.59 \cdot 10^{-4}$ | ±15.3 | ±20.3 | 2h00m45s |

computation time.

We compute the offsets in $(x_1, x_2)$ for the surfaces of cases A and B. For $\mathbf{\Phi} = \mathbf{0}$, we use $x_{i0} = \sqrt{2\beta_i I_i}$; the beta functions at $s = 0$ are given in TABLE II. For $J_1 = J_2 = 2 \cdot 10^{-7}$ m, case A, we find $x_{10} = 2.2$ mm and $x_{20} = 1.3$ mm. For $J_1 = J_2 = 4 \cdot 10^{-6}$ m, case B, we find $x_{10} = 10.8$ mm and $x_{20} = 6.1$ mm.

The approximate solutions can be sensitive to the mode set used for the calculation. As the set is increased, the likelihood of encountering a resonance increases and the whole technique can break down. For a suitable mode set, not so large as to spoil convergence, the Fourier amplitudes of $G_{\mathbf{\Phi}}$ appear to follow, with considerable scatter, a trend of exponential decrease with increasing $|m_1|$ and $|m_2|$ . One expects this for a function that is analytic in a strip about the real axis in the complex plane of $\Phi_1$ or $\Phi_2$. That is, the Fourier amplitudes of such a function should be bounded in modulus by an exponentially decreasing function of $|m_1|$ and $|m_2|$, and the rate of decrease is conditioned by the width of the strip. In KAM theory, $G_{\mathbf{\Phi}}$ is indeed analytic in strips. An argument based on analyticity is not

directly relevant in our approximation, however, since our $G_{\Phi}$ has only a finite number of modes and is analytic in the entire complex plane of $\Phi_i$.

In FIGs. 13 and 14, we give a logarithmic plot of the normalized modulus of Fourier amplitudes of $G_{\Phi_1}$, namely $|m_1 h(m_1, J_1, 0)|/J_1$ versus $|m_1|$ for two one-dimensional solutions, cases b and c of FIG. 6 and Table III. As expected, the magnitudes of the Fourier coefficients do not decay exactly exponentially, but roughly follow an exponential trend. Moreover, the rate of decrease of Fourier coefficients diminishes with increasing $J_1$, reflecting the general expectation and experience that more and more modes are needed for accurate computation of invariant surfaces at large actions.

For two-dimensional surfaces, the graphic representation of the decrease of the Fourier amplitudes with mode index is not as obvious as in the one-dimensional case. For a graphical display we have made a least-squares fit of the moduli of amplitudes, for cases A and B given in TABLE IV, to an exponential function, $|m_i h(\mathbf{m}, \mathbf{J}, 0)|/\|\mathbf{J}\| \approx C \exp(-a|m_1| - b|m_2|)$. In FIGs. 15–18, we plot the logarithms of the data and the fitted function (crosses and dashed line, respectively), versus $a|m_1| + b|m_2|$. As in the one-dimensional case, an exponential trend is evident, albeit with considerable scatter. Again, the decrease is slower at the relatively large action of FIGs. 17 and 18.

In this section, we have shown that the technique for solution of the Hamilton-Jacobi equation works well in non-integrable $s$-dependent cases with $d = 1$, even in regions of phase space close to domains of large scale instability. In similar cases with $d = 2$, it was difficult to approach such domains in reasonable computation time. Nevertheless, rather accurate invariant surfaces could be obtained under

conditions of substantial nonlinearity.

## VI. COMPARISON WITH OTHER WORK AND CONCLUSIONS

We have demonstrated a possible nonperturbative method for numerical solution of the Hamilton-Jacobi equation when the nonlinear perturbation is a periodic function of the independent variable, in particular a periodic step function. The primary goal of such a solution is to construct approximations to invariant tori. Consequently, any method that yields invariant tori, whether based on the Hamilton-Jacobi equation or not, should be evaluated in competition with the present method.

We have found that the technique described is quite expensive in computation time when applied for $d = 2$ at large amplitudes of oscillation, at least when high accuracy is required. This means that it is not very promising as it stands for a fully realistic model of accelerators, which must have $d = 3$ to allow for synchrotron oscillations as well as betatron oscillations. It is therefore imperative to find a more economical approach, either by improving the present method or by other means, if one is to study long-term stability of higher dimensional systems along the lines mentioned in the Introduction.

A well-established method in nonlinear mechanics is to work with the Poincaré return map, which takes a surface of section in phase space into itself. In this way one effectively eliminates one dimension of phase space, and one can hope that there are corresponding advantages in computational cost. In accelerator physics a convenient surface of section in the $(2d + 1)$-dimensional extended phase space

is defined by specifying a point on the reference orbit, say $s = 0$. The return map then propagates the other $2d$ phase space variables once around the ring, to $s = C$; it is called the "full-turn map". An invariant surface of the return map is a $d$-dimensional section of the $(d + 1)$-dimensional torus. It is represented by Eqn. (8)restricted to $s = 0$. This section of the full torus usually provides all necessary information on stability. In any case, the full torus is easily found from the section by a simple integration of the Hamilton-Jacobi equation with respect to $s$, taking $G_{\mathbf{\Phi}}(\mathbf{\Phi}, \mathbf{J}, s = 0)$ as initial condition.

We review two approaches to determination of invariants of the return map. In the first approach, which might be called the "many orbit picture", one states equations that an exact invariant surface or invariant function must satisfy. Describing the invariants by appropriate parameters, for instance Fourier or Taylor coefficients, one finds approximate solutions of the equations through perturbative or non-perturbative determination of the parameters. In the second approach, the "single orbit picture", one takes advantage of the fact that a single orbit is transitive on an invariant surface; i.e., it comes arbitrarily close to any point on the surface. Knowing the orbit, it should be possible to fit a surface to a subset of points on the orbit, again by determination of appropriate coefficients describing the surface. Notice that the many orbit and single orbit pictures correspond to the historical viewpoints based on partial and ordinary differential equations, respectively; that is, the Hamilton-Jacobi equation for consideration of all orbits at once, and the Hamilton equations for single orbits.

An obvious necessity in applying the return map method is to have a representation of the map that embodies the dynamics of the system with sufficient

accuracy. For studies of real laboratory systems such as complex accelerators, simple formulas for maps like those popular in the literature of nonlinear dynamics (standard map, quadratic map, etc.) are usually not adequate. One has to adopt formulas allowing greater complexity, for example a power series in Cartesian phase-space variables with a substantial number of terms,[22] or a finite Fourier series in angle variables with some flexible representation for the action dependence of the coefficients (say through polynomials or spline functions).[23] Such representations are being studied for accelerator theory,[22,23] along with necessary corrections to enforce the symplectic condition.[24,25] A more cautious and currently more reliable approach is to define the return map as the result of symplectic numerical integration through one period in $s$. In fact, formulas for maps are best derived as approximations to maps defined by symplectic integrators.

Let us first consider methods based on the many orbit picture. The requirement that a surface in phase space be left invariant by the return map can be formulated as a functional difference equation. As formulated by Moser in his original paper[3] on the Twist Theorem (KAM theorem for area-preserving maps of the plane), this is an equation for the canonical transformation that conjugates the map to a pure rotation. For proof of the Twist Theorem, Moser solved the equation by a sequence of transformations, using an algorithm that has come to be known as "super-convergent perturbation theory". Since the super-convergent perturbation theory is awkward to implement in numerical computation, it is interesting to consider either ordinary perturbation theory or nonperturbative methods for numerical solution of the functional equation.

There are at least two ways to formulate the functional equation, correspond-

ing to different ways of parametrizing the invariant surface.[26] If the surface is parametrized by the angle variable $\mathbf{\Phi}$ of the underlying integrable system, as in the representation of Eqn. (8), then the functional equation is quite analogous to the Hamilton-Jacobi equation, in that the constant action $\mathbf{J}$ is an input parameter, and $G_{\mathbf{\Phi}}$ (now evaluated at $s = 0$ only) is the unknown function. On the other hand, the surface may be parametrized by the new angle variable $\mathbf{\Psi}$, in which case the unknown is a pair of functions $\mathbf{J}(\mathbf{\Phi}, \mathbf{I}), \mathbf{\Psi}(\mathbf{\Phi}, \mathbf{I})$ defining the canonical transformation to new variables. This latter formulation gives Moser's equation, generalized to systems of arbitrary dimension.

Experience to date in nonperturbative solutions of the functional difference equations is quite limited. A program was written to solve the equation for $G_{\mathbf{\Phi}}$ for betatron motion with $d = 2$, for the same model that we treated here in Section 6. The results, reported briefly in Ref. 27 , confirmed that considerable computation time could be saved in comparison to the present method, even if the return map is represented by a symplectic integrator rather than by an explicit formula. Nonperturbative solutions of the generalized Moser equation would be interesting, but have not yet been attempted for $d = 2$. That equation allows, in principle, a better control of small divisors. In practice it gives a transformation that is not precisely canonical, however, since the transformation is obtained in explicit form rather than in the implicit form determined by a generating function.

When the map is given as a power series, the perturbative calculation of invariants of the return map may be cast in the language of Birkhoff normal forms, leading to a recursive algorithm that allows a practical generation of the perturbative series to rather high order.[28,29] In applications to accelerators this approach

has been much aided by a new method to compute the Taylor coefficients of the map,[22,28] given a symplectic integrator for the accelerator model at hand. The method uses automatic differentiation ("differential algebra") to generate derivatives of the map defined by the integrator, to machine precision.

A drawback in principle for this type of perturbation theory is that it aspires to compute an invariant function defined globally on phase space, rather than a single invariant surface. No such function exists in an exact sense, and the formal series for the function diverges. The series has an asymptotic character at best. Indeed, in practice one finds that computed invariants improve in quality initially, but finally deteriorate as the order of the calculation is increased. Since Moser's method aspires to find only an isolated invariant surface, on which invariant functions can be defined, it avoids this limitation in principle.

A more direct way to find a globally defined and approximately invariant function is to solve the defining equation of the function in a least-squares sense. If $z = (\mathbf{q}, \mathbf{p})$ is a point in phase space, an invariant function $K$ of the return map $\mathcal{M}$ is one such that $K(z) = K(\mathcal{M}(z))$. In Ref. 30, this equation was solved in a least-squares sense on a finite mesh in $z$-space, with $K$ represented as a linear combination of monomials in the components of $z$. For an example in 1 1/2 degrees of freedom, the Hénon map, it was found that curves around the origin and a fifth-order island chain could both be described by the same function.

Turning next to the single orbit approach, we consider the problem of determining a surface so that it passes through a subset of points on a single orbit of the return map. As in the case of functional equations, the fitting algorithm will depend on the choice of parametrization of the torus. Suppose that the torus is

parametrized as in Eqn. (8), so that the "curve parameter" is the unperturbed angle $\mathbf{\Phi}$. Then the problem can be stated as one of fitting a function $\mathbf{I}(\mathbf{\Phi})$, represented as a finite Fourier series, to orbit points $(\mathbf{I}(s), \mathbf{\Phi}(s)), s = 0 \pmod{C}$. An efficient method to perform such a fit was described in Ref. 31. When applied to the problem of Section V, at amplitudes $J_i$ close to those of Case D in Table IV, the method produces an invariant torus with *all* modes such that $|m_i| \leq M_i = 30$ in 2 minutes on the IBM 3090, versus 2 hours for the calculation of Table IV. Moreover, the calculation is much more accurate, since fewer modes were discarded; it gives $\delta_1 \approx 2 \times 10^{-7}, \quad \delta_2 \approx 2 \times 10^{-6}$. The fitted orbit was calculated by the same symplectic integrator used in Section V. A further saving in time might be attained by using an explicit formula for the map, rather than the integrator.

Since the Hamilton-Jacobi method seems uneconomical in comparison to surface fitting, is there any reason to consider it further for practical computations? There could very well be a reason, if the method of integrating the Hamilton-Jacobi equation with respect to $s$ could be made more efficient. Our primary interest in this paper was to show that the shooting method for $s$-periodicity is convergent and workable. We gave little attention to making the $s$-integration efficient, and in fact used a method that was familiar from earlier work but probably far from optimal. It involves making a $d$-dimensional Fourier transform and also an inverse Fourier transform, for every evaluation of the right-hand side of the ordinary differential equation (23); i.e., four such transform pairs for every Runge-Kutta step. These myriad transforms might be avoided by using values of $G$ on a mesh, rather than its Fourier coefficients, as unknowns. One has to enforce periodicity in $\mathbf{\Phi}$, but that might be done by using periodic B-splines to interpolate the function values. A

point in favor of the Hamilton- Jacobi shooting method is that it seems to have a bigger region of convergence than the analogous algorithm based on the functional equation.[27]

If the invariant surface is parametrized by the new angle $\mathbf{\Psi}$, conjugate to the constant action $\mathbf{J}$, then the surface to be fitted to orbit data at constant $\mathbf{J}$ is given by two finite Fourier series,

$$\mathbf{q}(\mathbf{\Psi},\mathbf{J}) = \sum_{\mathbf{m}\in\mathcal{S}} \mathbf{q_m}(\mathbf{J})e^{i\mathbf{m}\cdot\mathbf{\Psi}} \quad , \quad \mathbf{p}(\mathbf{\Psi},\mathbf{J}) = \sum_{\mathbf{m}\in\mathcal{S}} \mathbf{p_m}(\mathbf{J})e^{i\mathbf{m}\cdot\mathbf{\Psi}} \quad . \tag{52}$$

Here $(\mathbf{q},\mathbf{p})$ are globally defined phase-space coordinates; they could be Cartesian coordinates or angle-action variables of the underlying linear system; their values along orbits should be given directly by the return map. On a non-resonant orbit we should have $\mathbf{\Psi}(nC) = 2\pi\boldsymbol{\nu}n, \quad n = 0,1,\cdots$, for some tune $\boldsymbol{\nu}$ that has to be determined. Substituting this on the right-hand side of Eqn. (52), and orbit points $(\mathbf{q}(nC),\mathbf{p}(nC), \quad n = 0,1,\cdots)$ on the left-hand side, we get a set of equations to determine $\boldsymbol{\nu}$ and the Fourier coefficients $(\mathbf{q_m},\mathbf{p_m})$. Because $\boldsymbol{\nu}$ is initially unknown this is not a standard problem in Fourier analysis, backed up by a sound mathematical theory. Nevertheless, authors working in molecular dynamics,[32] plasma theory,[33] and celestial mechanics[34] have dealt with a similar problem in an heuristic way, by an adroit use of windowing functions with discrete Fourier transforms. It is not clear that the methods used to date are accurate and efficient enough for our purposes, especially for $s$-periodic perturbations in $d = 2$, but the problem would seem to deserve further investigation. The examples given in Refs. 32, 33, 34 are for autonomous systems with $d \leq 2$, thus considerably less difficult than our nonautonomous case with $d = 2$.

As is emphasized in Ref. 32, orbits close to resonances (within islands, in case $d = 1$) may lie on invariant surfaces that can be parametrized as in Eqn. (52), always with the same choice of $(\mathbf{q}, \mathbf{p})$. By contrast, the representation (8) is useful only for surfaces that "surround the origin", i.e., that can be deformed continuously into surfaces $\mathbf{I}$=constant, $\mathbf{\Phi} \in [0, 2\pi]^d$. To treat surfaces associated with resonances by our methods, one has to make a preliminary change of coordinates, and some dynamical information is required to choose those coordinates. Moreover, in the Poincaré framework, one may be seeking invariant surfaces of higher powers of the return map, rather than of the map itself.

The foregoing brief review, which is far from comprehensive, should give the impression that the question of how best to compute invariant surfaces is not a closed subject, particularly when the surfaces in question do not surround the origin. The present study adds a new entry to the list of possible techniques for studying this long standing problem.

## ACKNOWLEDGEMENTS

One of the authors (W. E. G.) would like to thank John Cary of the University of Colorado for his support and the Accelerator Theory and Special Projects group at SLAC for their hospitality. This work was supported by the Department of Energy contracts DE-FG02-86ER40302 (Colorado) and DE-AC03-76SF00515 (SLAC).

# APPENDIX I. CONVERGENCE OF THE SHOOTING METHOD

In this appendix we discuss the convergence properties of the shooting algorithm, as realized by solving the fixed point problem (29) through simple iteration. We show that under certain restrictions the iteration is governed by the contraction mapping theorem[35]. It follows that there exists a unique fixed point of $A$ in a certain metric space. The argument is valid only when the set of Fourier modes of the generating function is finite, and includes no resonant mode.

Recall that the fixed point problem, $h_0 = A(h_0)$, has the following form expressed in terms of vector components labeled by the mode index $\mathbf{m}$:

$$h_0(\mathbf{m}) = \frac{1}{e^{2\pi i \mathbf{m}\cdot\boldsymbol{\nu}} - 1} \int_0^C ds f(\mathbf{m}, h(s; h_0), s) \quad , \tag{53}$$

where the function $f$ is defined by

$$f(\mathbf{m}, h(s; h_0), s) =$$
$$-e^{i\mathbf{m}\cdot\mathbf{X}(s)} \int_0^{2\pi} \left[\frac{d\boldsymbol{\Phi}}{2\pi}\right] e^{-i\mathbf{m}\cdot\boldsymbol{\Phi}} V\left(\boldsymbol{\Phi}, \mathbf{J} + \sum_{\mathbf{n}} i\mathbf{n} h(\mathbf{n}, s; h_0) e^{i\mathbf{n}\cdot(\boldsymbol{\Phi} - \mathbf{X}(s))}, s\right) \quad , \tag{54}$$

and $h(\mathbf{m}, s; h_0)$ is the solution of the following differential equation with initial condition $h_0$:

$$\frac{dh(\mathbf{m}, s; h_0)}{ds} = f(\mathbf{m}, h(s; h_0), s) \quad . \tag{55}$$

To indicate that a function depends on an entire vector having components labeled by the mode index, we suppress reference to the index.

# A. Model Problem

For the discussion of contractive properties, we consider an analogous problem with a complex $h_0$ that has only a single component (mode). We thereby simplify the notation without losing any essential features. A later generalization to cover the full system with many modes will be immediate. The equations for the model fixed point problem take the form

$$h_0 = \frac{1}{D}\int_0^C ds f\Big(h(s;h_0),s\Big) \quad , \tag{56}$$

$$\frac{dh}{ds}(s;h_0) = f\Big(h(s;h_0),s\Big) \quad . \tag{57}$$

with $h(0;h_0) = h_0$. The dependence of the solution of the differential equation on the initial condition is displayed explicitly. The small divisor is represented by $D$ and is analogous to the divisor, $\exp(2\pi i\mathbf{m}\cdot\boldsymbol{\nu}) - 1$, that appears in Eqn. (53).

The contraction mapping theorem, which will be applied at two different levels to solve this problem, is as follows. Suppose that an operator $F$ maps a complete metric space $\mathcal{S}$ into itself, and is contractive on $\mathcal{S}$. Then there exists a unique fixed point $x = F(x)$ in $\mathcal{S}$. Moreover, $x$ may be computed by iteration, $x^{(p+1)} = F(x^{(p)})$, where $x^{(0)}$ is any element of $\mathcal{S}$. The contraction condition is that

$$d(F(x_1),F(x_2)) \leq \alpha d(x_1,x_2) \quad , \tag{58}$$

for all $x_1, x_2 \in \mathcal{S}$ and a fixed $\alpha \in (0,1)$. Here $d(x_1,x_2)$ is the distance between $x_1$ and $x_2$ in the metric of $\mathcal{S}$, and the iteration converges to the solution $x$ in the sense $d(x^{(p)},x) = \mathcal{O}(\alpha^p)$.

We suppose that the complex function $f(h,s)$ is piecewise-continuous as a function of $s$ on $[0,C]$, and is bounded and Lipschitz-continuous as a function of $y$, as follows:

$$\begin{aligned} |f(y,s)| &< f_0 \quad , \\ |f(y_1,s) - f(y_2,s)| &< f_1 |y_1 - y_2| \quad , \\ |y|, |y_1|, |y_2| &< r \quad , \quad s \in [0,C] \quad . \end{aligned} \tag{59}$$

The positive constants $r, f_0, f_1$ will be restricted to meet the requirements of the proof.

## B. Solution of the Differential Equation

We first discuss existence and uniqueness of solutions to the differential equation (57), and estimate the dependence of a solution on the initial condition. We work with the equivalent integral equation. After the substitution $x(s) = h(s;h_0) - h_0$ it has the form

$$x(s) = \int_0^s d\sigma f(x(\sigma) + h_0, \sigma) \quad , \tag{60}$$

or $x = F(x)$ with the integral operator $F$ defined by the right hand side of (60).

For analysis of (60) by the contraction mapping principle, the complete metric space $\mathcal{S}$ will be a ball $\|x\| < r_1$ in the Banach space of all continuous complex functions $x(s)$ on $[0,C]$ with norm $\|x\| = \sup_{s\in[0,C]} |x(s)|$; the distance is $d(x_1,x_2) = \|x_1 - x_2\|$. Suppose that $|h_0| < r_0$. Then $F$ will take $\mathcal{S}$ into itself if

$$(i) \quad r_0 + r_1 < r$$

$$(ii) \quad \hat{C} f_0 < r_1 \tag{61}$$

Here $\hat{C}$ is the sum of the lengths of intervals within $[0, C]$ on which $f(y, s)$ is non-zero. (Recall that in the accelerator problem, the analogous function is non-zero only over the extent of sextupoles, so that $\hat{C}$ is much less than $C$ itself). Conditions (61) are evidently sufficient, since

$$\begin{aligned} |x(s)| &\leq \int_0^s d\sigma \, |f(x(\sigma) + h_0, \sigma)| \\ &\leq \hat{C} \sup_{s \in [0,C]} |f(x(s) + h_0, s)| \\ &\leq \hat{C} f_0 \quad , \end{aligned} \tag{62}$$

if $|x(s) + h_0| < r$, whereas $|x(s) + h_0| \leq |x(s)| + |h_0| < r_1 + r_0$.

To show that $F$ is contractive on $\mathcal{S}$, assume that $\|x_1\|, \|x_2\| < r_1$ and note that

$$|F(x_1, h_0)(s) - F(x_2, h_0)(s)| \leq \int_0^s d\sigma |f(x_1(\sigma) + h_0, \sigma) - f(x_2(\sigma) + h_0, \sigma)|$$

$$\leq f_1 \int_0^s d\sigma |x_1(\sigma) - x_2(\sigma)| \leq \hat{C} f_1 \|x_1 - x_2\| \quad , \tag{63}$$

if $|x_i(\sigma) + h_0| < r$, which is implied by (61). The contraction condition is guaranteed by adding the condition

$$(iii) \quad \hat{C} f_1 < 1 \tag{64}$$

For later account of the boundary condition, we have to know how the solution of the differential equation depends on the initial condition $h_0$. Suppose that

$|h_{0i}| < r_0$ and $|x(s;h_{0i})| < r_1, i = 1,2$ and form the difference

$$h(s;h_{01}) - h(s;h_{02}) = h_{01} - h_{02} + \int_0^s d\sigma \left[ f(h(\sigma;h_{01}),\sigma) - f(h(\sigma;h_{02}),\sigma) \right] \quad . \quad (65)$$

Since $|h(\sigma;h_{0i})| < r$ we have

$$|h(s;h_{01}) - h(s;h_{02})| \leq |h_{01} - h_{02}| + f_1 \hat{C} \sup_\sigma |h(\sigma;h_{01}) - h(\sigma;h_{02})| \quad , \quad (66)$$

thus

$$\|h(\cdot;h_{01}) - h(\cdot;h_{02})\| \leq \frac{|h_{01} - h_{02}|}{1 - f_1 \hat{C}} \quad , \quad (67)$$

in view of Eq.(64).

## C. Solution of the Fixed Point Problem

Having learned enough about solutions of the differential equation, we can now apply the contraction mapping principle to solve the one-dimensional fixed point problem (56) for the initial condition $h_0$ that meets the boundary condition. Here the complete metric space $\mathcal{S}$ is a disk in the complex plane, all complex numbers $z$ with $|z| < r_0$. We assume the conditions $(i), (ii), (iii)$ derived above, so that the solution of the differential equation satisfies $|x(s;h_0)| < r_1$ with $|h_0| < r_0$, and condition (67).

If $|h_0| < r_0$, then

$$|A(h_0)| \leq \left| \frac{1}{D} \int_0^C ds f(x(s;h_0) + h_0, s) \right| < \frac{\hat{C}}{|D|} f_0 \quad , \quad (68)$$

which is to say that $A$ maps $\mathcal{S}$ into itself provided that

$$(iv) \quad \frac{\hat{C}}{|D|} f_0 < r_0 \tag{69}$$

Finally we verify the contraction condition, with the help of (67). Supposing that $|h_{01}|, |h_{02}| < r_0$ we have

$$\begin{aligned} |A(h_{01}) - A(h_{02})| &\leq \frac{1}{|D|} \int_0^C ds |f(h(s; h_{01}), s) - f(h(s; h_{02}), s)| \\ &\leq \frac{f_1 \hat{C}}{|D|} \sup_s |h(s; h_{01}) - h(s; h_{02})| \\ &\leq \frac{f_1 \hat{C}}{|D|} \frac{1}{1 - f_1 \hat{C}} |h_{01} - h_{02}| \end{aligned} \tag{70}$$

The operator is contractive if the coefficient of $|h_{01} - h_{02}|$ is less than one, or

$$(v) \quad \frac{\hat{C} f_1}{|D|} < \frac{1}{1 + |D|} \tag{71}$$

To summarize, under the conditions on $f$ stated in Subsection A there is a unique solution of our problem with $\|x\| < r_1$ and $|h_0| < r_0$ provided that conditions $(i)$ through $(v)$ hold. If $f(y, s)$ contains an adjustable multiplicative constant, like the sextupole strength in the example of Section V, then the constant can be adjusted to make $f_0$ and $f_1$ so small as to satisfy all the conditions $(i) - (v)$.

## D. The Original Problem

The original problem defined by (53) and (54) can be treated in close analogy to the model problem. Now $f$ is a vector, with components labeled by the mode index $\mathbf{m}$, and has a vector argument with similarly labeled components. Boundedness and continuity conditions are as follows:

$$
\begin{aligned}
|f(\mathbf{m}, y, s)| &< f_0 \quad , \\
|f(\mathbf{m}, y_1, s) - f(\mathbf{m}, y_2, s)| &< f_1 \|y_1 - y_2\| \quad , \\
\mathbf{m} \in \mathcal{M} \quad , \quad \|y\|, \|y_1\|, \|y_2\| &< r \quad , \quad s \in [0, C] \quad .
\end{aligned} \tag{72}
$$

The norms for the extended spaces are defined in the obvious way,

$$
\|y\| = \sup_{\mathbf{m},s} |y(\mathbf{m}, s)| \quad , \quad \|h_0\| = \sup_{\mathbf{m}} |h_0(\mathbf{m})| \quad . \tag{73}
$$

It is now easy to check that all the steps of the proof for the model problem go through for the full problem under conditions (72), if one merely takes the supremum over $\mathbf{m}$ as well as $s$, whenever a norm is to be estimated. We of course require that there be no resonant modes within the finite set of modes allowed, and define $|D|$ as the minimum value of the small divisor:

$$
|e^{2\pi i \mathbf{m} \cdot \boldsymbol{\nu}} - 1| \geq |D| \quad . \tag{74}
$$

To complete the argument, we have to find conditions on the Hamiltonian perturbation $V$ such that requirements (72) will be met. We assume that $V(\boldsymbol{\Phi}, \mathbf{J}, s)$ is continuous in $\boldsymbol{\Phi} \in [0, 2\pi]$, piecewise continuous in $s \in [0, C]$, and has a continuous

derivative with respect to $\mathbf{J}$ in a region to be specified presently. Sums on mode numbers $\mathbf{m}$ run over the set $M \cup \bar{M}$; let $\mathcal{N}$ be the number of elements in this set, and $\mathcal{M}$ the largest value of $|m_j|$ for elements of the set. Then

$$\sup_{\mathbf{\Phi},s}\Big|\sum_{\mathbf{m}} im_j y(\mathbf{m},s)e^{i\mathbf{m}\cdot(\mathbf{\Phi}-\mathbf{X}(s))}\Big| \leq \mathcal{M}\mathcal{N}\|y\| \quad , \tag{75}$$

and by (54) the first inequality of (72) will hold if

$$\sup_{\mathbf{\Phi},s} |V(\mathbf{\Phi},\mathbf{J}+\mathbf{K},s)| < f_0 \quad , \quad |K_j| < \mathcal{M}\mathcal{N}r \quad . \tag{76}$$

By the mean value theorem,

$$\begin{aligned} &|f(\mathbf{m},y_1,s) - f(\mathbf{m},y_2,s)| \\ &\leq \sup_{\mathbf{\Phi},s} |V(\mathbf{\Phi},\mathbf{J}+\mathbf{K}_1,s) - V(\mathbf{\Phi},\mathbf{J}+\mathbf{K}_2,s)| \\ &\leq \sup_{\mathbf{\Phi},\mathbf{K},s} \sum_j |V_{J_j}(\mathbf{\Phi},\mathbf{J}+\mathbf{K},s)|\,|K_{1j}-K_{2j}| \quad , \end{aligned} \tag{77}$$

where

$$K_{pj} = \sum_{\mathbf{m}} im_j y_p(\mathbf{m},s)e^{i\mathbf{m}\cdot(\mathbf{\Phi}-\mathbf{X}(s))} \quad , \tag{78}$$

and the supremum with respect to $\mathbf{K}$ is over $|K_j| \leq \max\big[|K_{1j}|,|K_{2j}|\big] \leq \mathcal{M}\mathcal{N}r$. Since $|K_{1j}-K_{2j}| \leq \mathcal{M}\mathcal{N}\|y_1-y_2\|$, we verify the second inequality of (72) if

$$\mathcal{M}\mathcal{N}d \sup_{j,\mathbf{\Phi},s} |V_{J_j}(\mathbf{\Phi},\mathbf{J}+\mathbf{K},s)| < f_1 \quad , \quad |K_j| < \mathcal{M}\mathcal{N}r \quad , \tag{79}$$

where $d$ is the number of degrees of freedom.

Thus, apart from reasonable conditions of continuity, our main sufficient conditions for the shooting method to succeed are that $V$ and $dV/d\mathbf{J}$ be sufficiently small. Of course, the conditions we have derived are very far from necessary, being based on pessimistic upper bounds. The point of the above discussion is to show that the shooting algorithm has a solid theoretical basis, at least under favorable circumstances.

## REFERENCES


1. A. M. Perelomov, *Integrable Systems of Classical Mechanics and Lie Algebras*, (Birkhauser, Basel, Switzerland, 1990).

2. *Soliton Theory: a Survey of Results*, edited by A. P. Fordy (Manchester Univ. Press, Manchester, 1990).

3. V. I. Arnol'd, Russ. Math. Surveys **18:6**, 85 (1963); J. Moser, Nachr. Akad. Wiss. Göttingen, Math. Phys. Kl. (1962); A. N. Kolmogorov, Dokl. Akad. Nauk. SSSR **98**, 525 (1954), English version in *Proc. of the 1954 Int. Cong. of Math.*, (North-Holland, Amsterdam, 1957). A good general reference is G. Gallavotti, *The Elements of Mechanics*, (Springer, New York, 1983).

4. V. I. Arnol'd, Sov. Math.—Doklady **5**, 581 (1964)

5. R. L. Warnock and R. D. Ruth, Physica **26D**, 1 (1987).

6. R. L. Warnock and R. D. Ruth, Phys. Rev. Lett. **66**, 990 (1991); SLAC report SLAC-PUB-5267, July, 1991, to be published in Physica D; in *Proc. Workshop on Nonlinear Problems in Future Particle Accelerators, Capri,*

*Italy, 19-25 April, 1990*, edited by W. Scandale and G. Turchetti (World Scientific, Singapore, 1991).

7. N. N. Nekhoroshev, Russian Math. Surveys **32**, 1 (1977).

8. William E. Gabella, Ph. D. thesis, University of Colorado, Boulder, 1991.

9. W. E. Gabella, R. D. Ruth, and R. L. Warnock, in *Nonlinear Dynamics and Particle Acceleration, Tsukuba, Japan, 1990*, AIP Conf. Proc. **230**, edited by T. Tajima and Y. Ichikawa (Amer. Inst. Phys., New York, 1991); in *Proc. 1989 IEEE Particle Accelerator Conference, March 20-23, 1989, Chicago*, edited by F. Bennett and J. Kopta (IEEE, New York, 1989); in *Proc. Second Advanced ICFA Beam Dynamics Workshop, Lugano, Switzerland, April 11-16, 1988*, edited by J. Hagel and E. Keil, CERN report CERN 88-04, 1988.

10. R. D. Ruth, in *Nonlinear Dynamics Aspects of Particle Accelerators*, Lect. Notes in Phys. **247**, edited by J. M. Jowett *et al.*, (Springer, Berlin, 1986), pp. 37–63.

11. E. D. Courant and H. S. Snyder, Ann. Phys. (N. Y.) **3**, 1 (1958).

12. H. Goldstein, *Classical Mechanics* (Addison-Wesley, Reading, MA, 1980).

13. M. A. Krasnosel'skii *et al.*, *Approximate Solutions of Operator Equations*, (Woltors- Noordhoff, Groningen, 1972).

14. G. Dahlquist and A. Bjorck, *Numerical Methods*, (Prentice-Hall, Inc., 1974).

15. C. G. Broyden, Math. Comp. **19**, 577 (1965).

16. J. E. Dennis, Jr., Math. Comp. **25**, 559 (1971).

17. M. J. Powell, in *Proc. of the First Int. Conf. on Industrial and Applied Math.*, edited by J. Meckenna and R. Terman, (SIAM, Philadelphia, 1988).

18. E. Keil, in *Theoretical Aspects of the Behavior of Beams in Accelerators and Storage Rings*, CERN report CERN 77–13, 1977

19. *1-2 GeV Synchrotron Radiation Source, Conceptual Design Report–July, 1986*, PUB-5172 rev., (Lawrence Berkeley Laboratory, Berkeley, California).

20. R. Ruth, CERN report CERN-LEP/TH/83-14 (1983); É. Forest and R. D. Ruth, Physica **43 D**, 105 (1990).

21. M. A. Furman and S. G. Peggs, SSC report SSC-N-634, 1989.

22. M. Berz, SSC report SSC-152 (1988); R. Kleiss, F. Schmidt, Y. Yan, and F. Zimmermann, CERN report CERN SL/92-02 (AP) (1992).

23. R. L. Warnock, in *Proc. 1989 IEEE Particle Accelerator Conf., loc. cit.*, p.1332.

24. J. Irwin, SSC report SSC-228 (1989).

25. J. S. Berg and R. L. Warnock, in *Proc. 1991 Particle Accelerator Conf., May 6-9, 1991, San Francisco*, edited by L. Lizama and J. Chew, p. 1654 (IEEE, New York, 1991).

26. R. L. Warnock, in *Nonlinear Dynamics and Particle Acceleration*, AIP Conf. Proc. No. **230** (AIP, New York, 1991).

27. R. L. Warnock and R. D. Ruth, in *Proc. Third Advanced ICFA Beam Dynamics Workshop*, Novosibirsk, USSR, May 29 - June 2, 1989 (Inst. Nuc. Phys., Novosibirsk, 1989); available as SLAC report No. SLAC-PUB-5020.

28. É. Forest, M. Berz, and J. Irwin, Part. Accel. **24** (1987) 91, and unpublished computer codes of Forest *et al.*

29. G. Turchetti, in *Nonlinear Problems in Future Particle Accelerators, loc. cit.*

30. A. Bazzani, E. Remiddi, and G. Turchetti, J. Phys. A: Math. Gen. **24** (1991) L53.

31. R. L. Warnock, Phys. Rev. Lett. **66**, 1803 (1991).

32. C. C. Martens and G. S. Ezra, J. Chem. Phys. **86**, 279 (1987).

33. A. H. Reiman and N. Pomphrey, J. Comput. Phys., to be published.

34. J. Binney and D. Spergel, Astrophys. J. **252**, 308 (1982).

35. M. S. Berger, *Nonlinearity and Functional Analysis* (Academic Press, New York, 1977) pp. 112–113. Y. Choquet-Bruhat, C. DeWitt-Morette, and M. Dillart-Bleick, *Analysis, Manifolds and Physics* (North-Holland, Amsterdam, 1982) pp. 88–90.

# Figure Captions

FIG. 1. The $I_1/I_{1u}$ surface for linear coupling with strength $\Gamma = 0.65$ m$^{-2}$.

FIG. 2. The $I_2/I_{2u}$ surface for linear coupling with strength $\Gamma = 0.65$ m$^{-2}$.

FIG. 3. The normalized tuneshifts $\Delta\nu_1^{HJ}/K$ as a function of the normalized quadrupole strength. The dotted line is the analytic result, and the ($\times$) mark data from numerical solution of the Hamilton-Jacobi equation.

FIG. 4. The normalized tuneshifts $\Delta\nu_2^{HJ}/K$ as a function of the normalized quadrupole strength. The dotted line is the analytic result, and the ($\times$) mark data from numerical solution of the Hamilton-Jacobi equation.

FIG. 5. Initial actions $\mathbf{I}(\mathbf{\Phi} = 0, s = 0)$ of trajectories stable ($\cdot$) and unstable ($\star$) after tracking for 5000 turns in the ALS cell. The points A through D mark two-dimensional solutions that are discussed in some detail in the text.

FIG. 6. Approximate one-dimensional invariant curves $I_1(\Phi_1, J_1, 0)$ found from the numerical solution of the Hamilton-Jacobi equation. The angle variable is normalized by $2\pi$. See TABLE III and text for details.

FIG. 7. Contours of constant nonlinear tune shift $1000 \cdot \Delta\nu_1$. Points where numerical solutions were found and used in the global fit are marked with $\times$.

FIG. 8. Contours of constant nonlinear tune shift $1000 \cdot \Delta\nu_2$. Points where numerical solutions were found and used in the global fit are marked with $\times$.

FIG. 9. The $I_1(\mathbf{\Phi}, \mathbf{J}, 0)/J_1$ projection of the invariant surface for $J_1 = J_2 = 2 \cdot 10^{-7}$ m. This corresponds to A in FIG. 5 and in TABLE IV.

FIG. 10. The $I_2(\mathbf{\Phi}, \mathbf{J}, 0)/J_2$ projection of the invariant surface for $J_1 = J_2 = 2 \cdot 10^{-7}$ m. This corresponds to A in FIG. 5 and in TABLE IV.

FIG. 11. The $I_1(\mathbf{\Phi}, \mathbf{J}, 0)/J_1$ projection of the invariant surface for $J_1 = J_2 = 4 \cdot 10^{-6}$ m. This corresponds to B in FIG. 5 and in TABLE IV.

FIG. 12. The $I_2(\mathbf{\Phi}, \mathbf{J}, 0)/J_2$ projection of the invariant surface for $J_1 = J_2 = 4 \cdot 10^{-6}$ m. This corresponds to B in FIG. 5 and in TABLE IV.

FIG. 13. Modulus of Fourier amplitudes of one-dimensional surfaces shown in FIG. 6 with $J_1 = 2 \cdot 10^{-5}$ m, case c. Notice the fast decrease of the Fourier amplitudes with mode number typical of good solutions.

FIG. 14. Modulus of Fourier amplitudes of one-dimensional surfaces shown in FIG. 6 with $J_1 = 2 \cdot 10^{-6}$ m, case b.

FIG. 15. Decrease of the Fourier amplitudes with mode number for $J_1 = J_2 = 2 \cdot 10^{-7}$ m—case A of TABLE IV. The figure shows values of $\log(|m_1 h|/\sqrt{J_1^2 + J_2^2})$, indicated by crosses, plotted versus $a|m_1| + b|m_2|$ with $a = 0.396$ and $b = 0.485$. The constants $a$ and $b$ were determined by a least squares fit to the function $\log C - a|m_1| - b|m_2|$, which is plotted as a dashed line.

FIG. 16. Decrease of the Fourier amplitudes with mode number for $J_1 = J_2 = 2 \cdot 10^{-7}$ m—case A of TABLE IV. The figure shows values of $\log(|m_2 h|/\sqrt{J_1^2 + J_2^2})$, indicated by crosses, plotted versus $a|m_1| + b|m_2|$ with $a = 0.493$ and $b = 0.438$. The constants $a$ and $b$ were determined by a least squares fit to the function $\log C - a|m_1| - b|m_2|$, which is plotted as a dashed line.

FIG. 17. Decrease of the Fourier amplitudes with mode number for $J_1 = J_2 = 4 \cdot 10^{-6}$ m—case B of TABLE IV. The figure shows values of $\log(|m_1 h|/\sqrt{J_1^2 + J_2^2})$, indicated by crosses, plotted versus $a|m_1| + b|m_2|$ with $a = 0.0456$ and $b = 0.154$. The constants $a$ and $b$ were determined by a least-squares fit to the function $\log C - a|m_1| + b|m_2|$, which is plotted as a dashed line.

FIG. 18. Decrease of the Fourier amplitudes with mode number for $J_1 = J_2 = 4 \cdot 10^{-6}$ m—case B of TABLE IV. The figure shows values of $\log(|m_2 h|/\sqrt{J_1^2 + J_2^2})$, indicated by crosses, plotted versus $a|m_1| + b|m_2|$ with $a = 0.107$ and $b = 0.0999$. The constants $a$ and $b$ were determined by a least-squares fit to the function $\log C - a|m_1| + b|m_2|$, which is plotted as a dashed line.

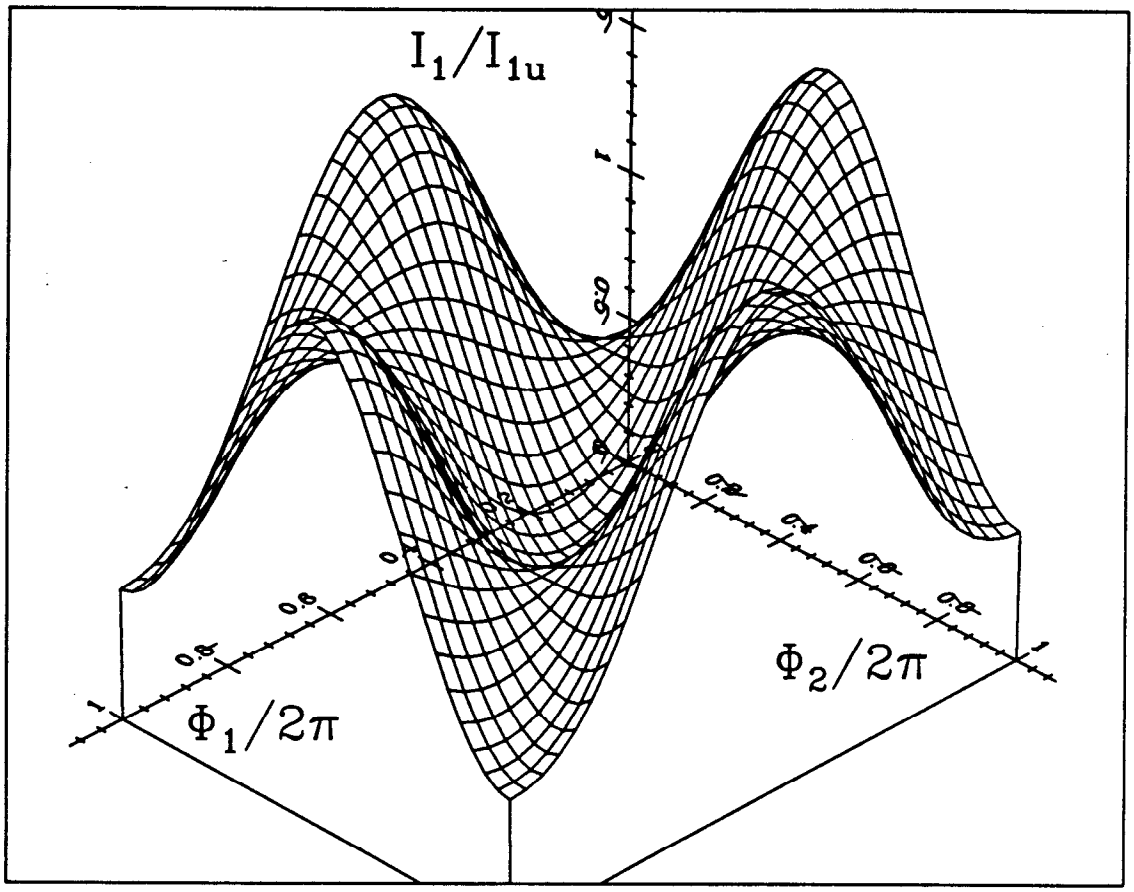


Fig. 1

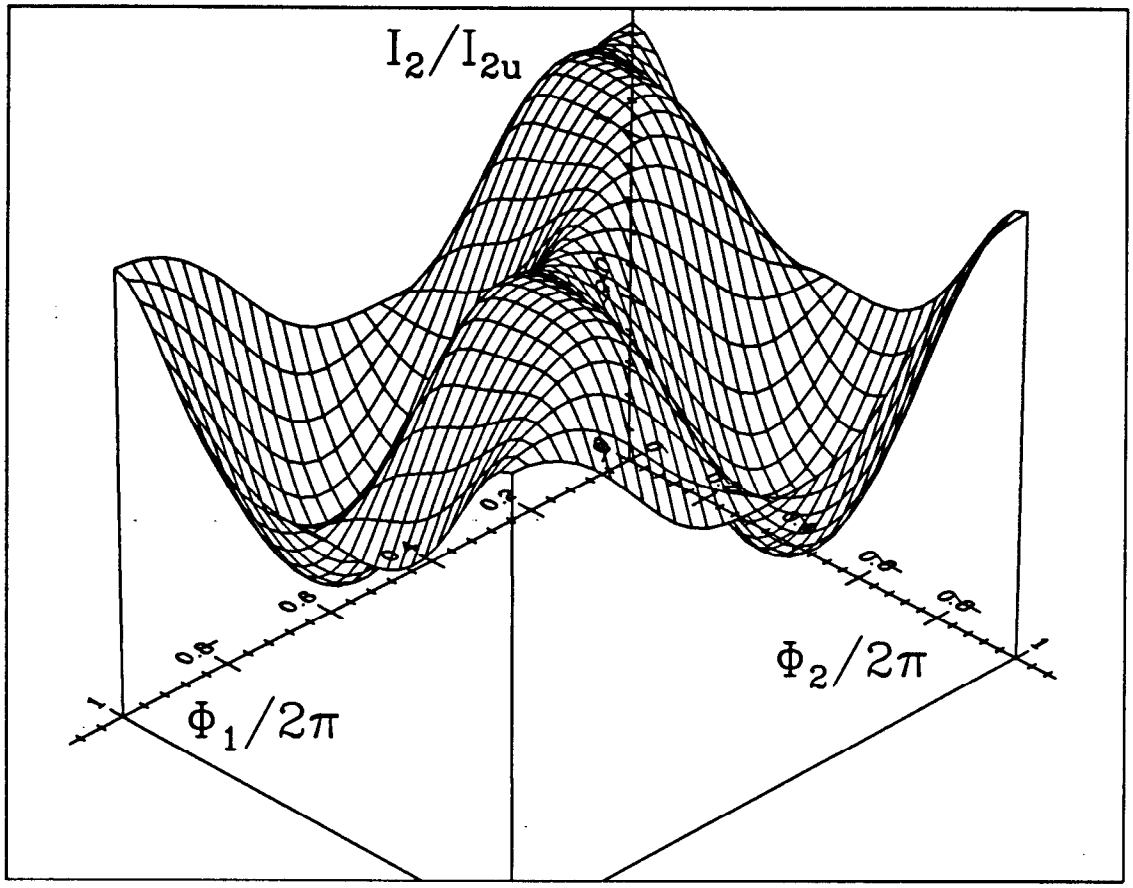


Fig. 2

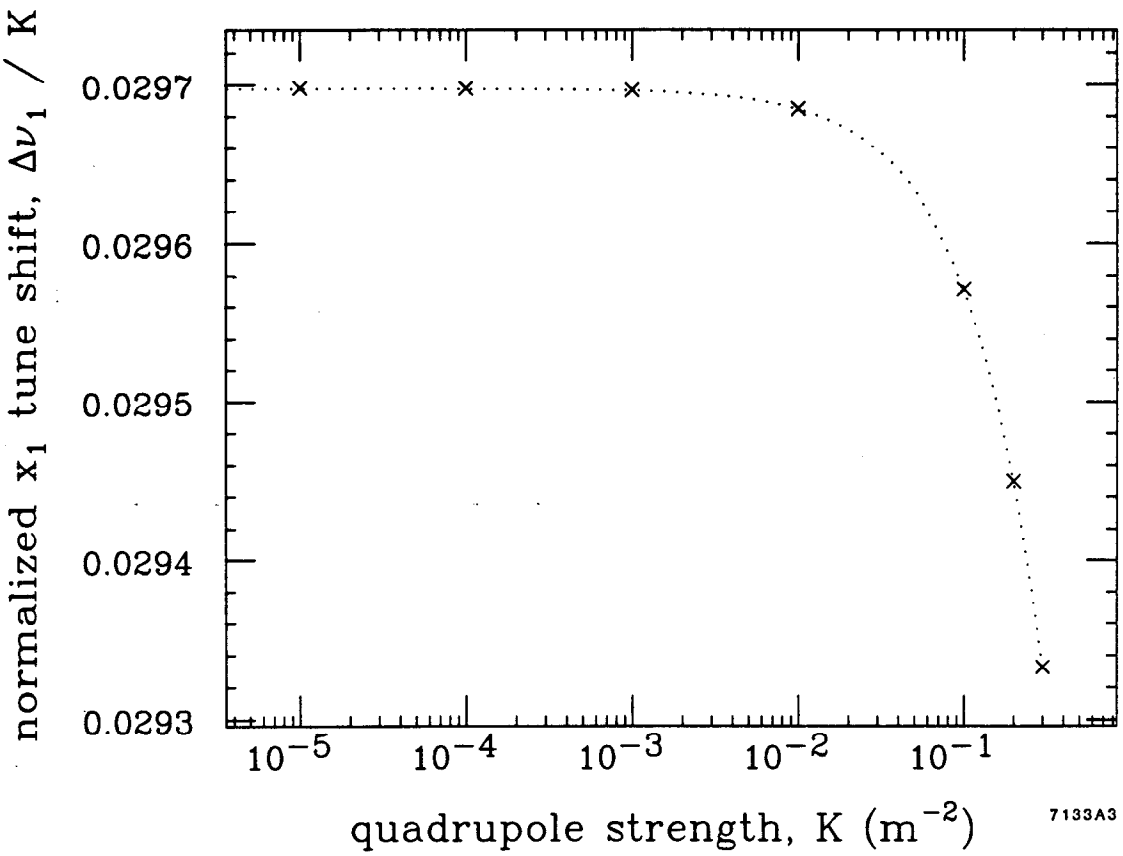
normalized $x_1$ tune shift, $\Delta\nu_1$ / K
0.0297
0.0296
0.0295
0.0294
0.0293
$10^{-5}$
$10^{-4}$
$10^{-3}$
$10^{-2}$
$10^{-1}$
quadrupole strength, K ($m^{-2}$)
7133A3

Fig. 3

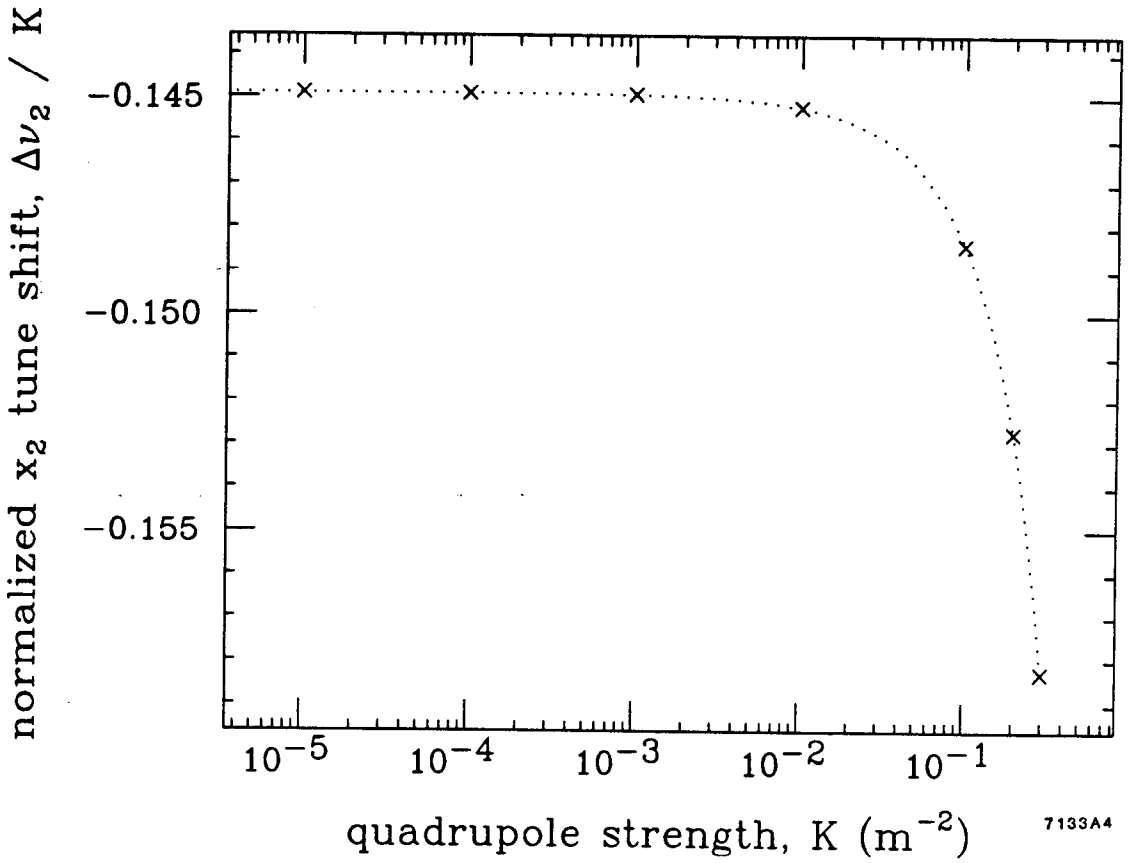
normalized $x_2$ tune shift, $\Delta\nu_2$ / K
−0.145
−0.150
−0.155
$10^{-5}$
$10^{-4}$
$10^{-3}$
$10^{-2}$
$10^{-1}$
quadrupole strength, K ($m^{-2}$)
7133A4

Fig. 4

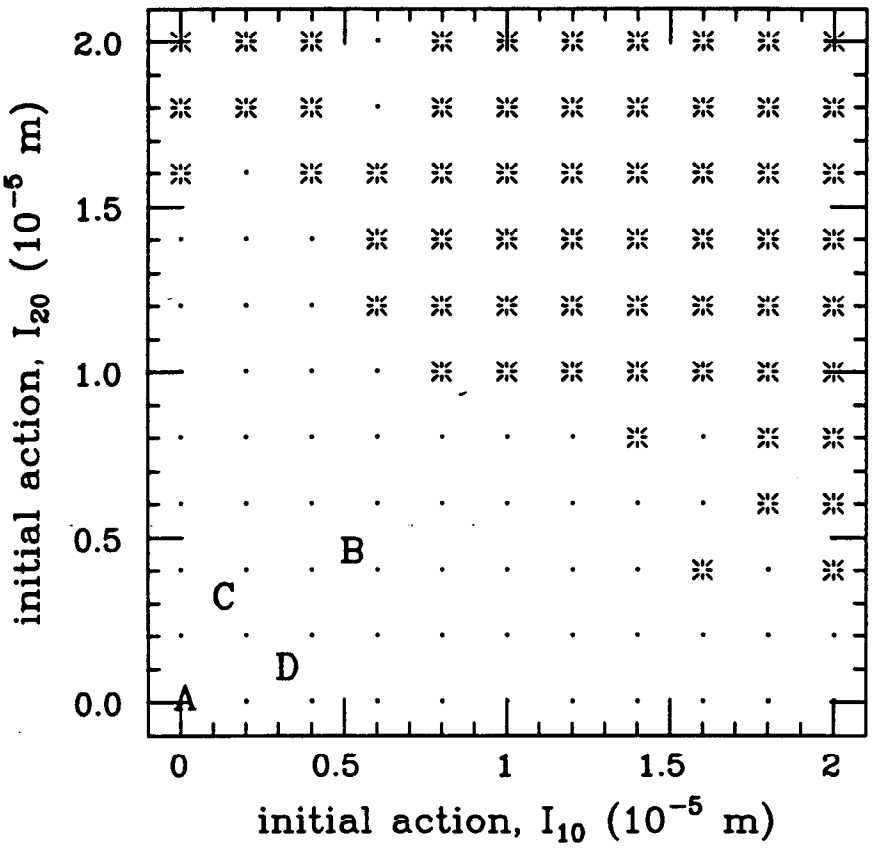
2.0
1.5
1.0
0.5
0.0
initial action, $I_{20}$ ($10^{-5}$ m)
A
B
C
D
0
0.5
1
1.5
2
initial action, $I_{10}$ ($10^{-5}$ m)
7133A5

Fig. 5

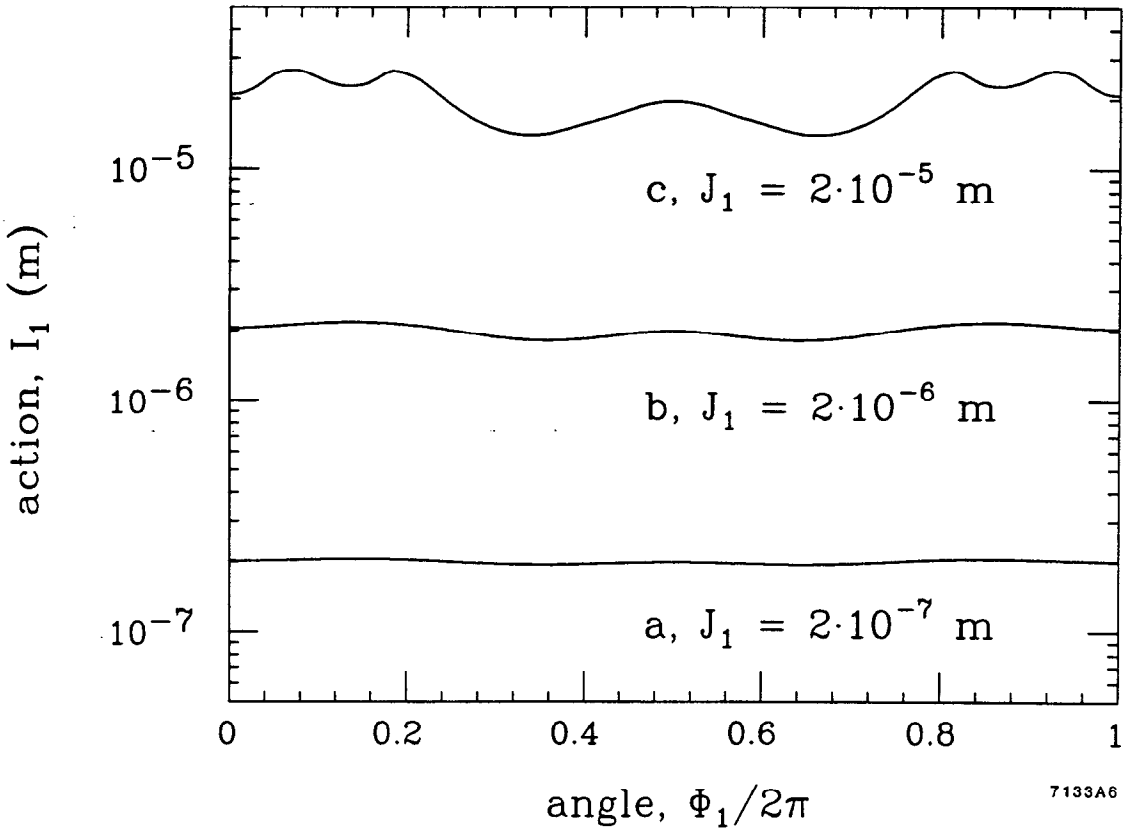
action, $I_1$ (m)
$10^{-5}$
$10^{-6}$
$10^{-7}$
c, $J_1 = 2 \cdot 10^{-5}$ m
b, $J_1 = 2 \cdot 10^{-6}$ m
a, $J_1 = 2 \cdot 10^{-7}$ m
0
0.2
0.4
0.6
0.8
1
angle, $\Phi_1/2\pi$
7133A6

Fig. 6

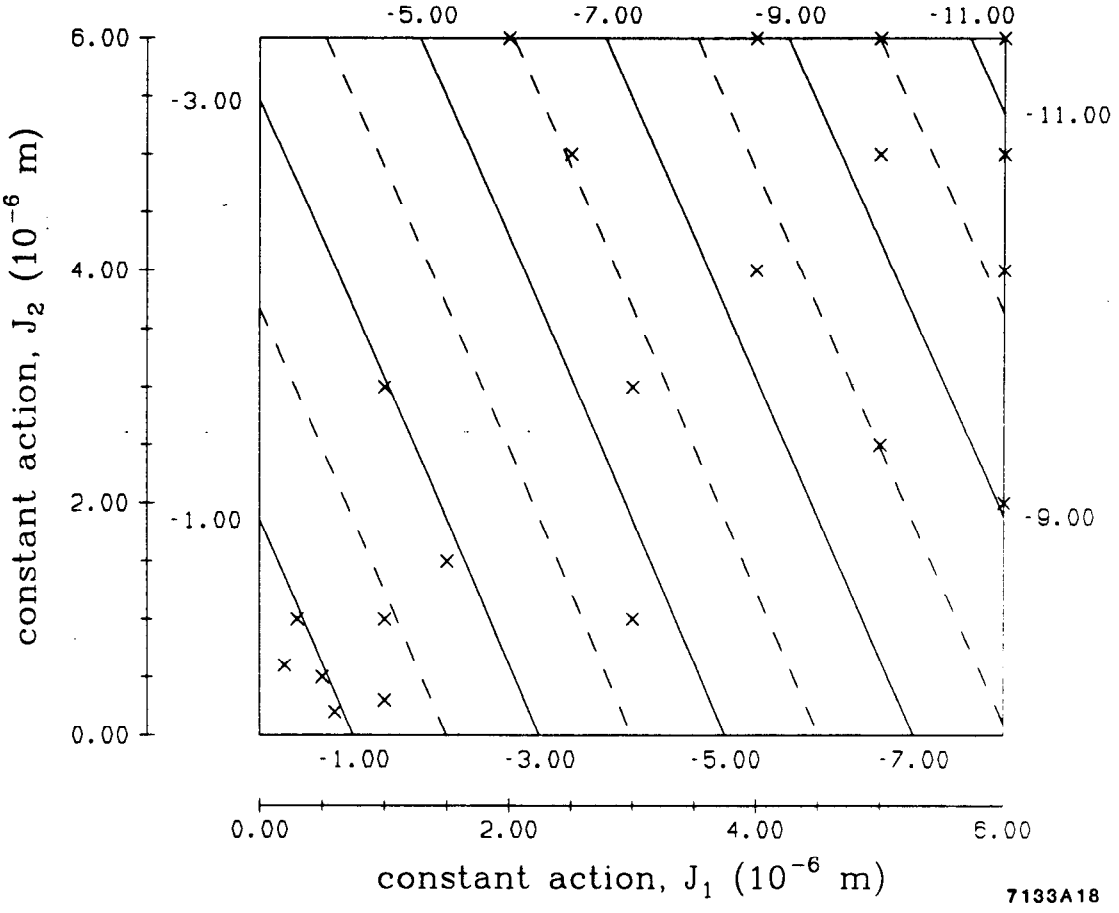
-5.00
-7.00
-9.00
-11.00
6.00
-3.00
-11.00
4.00
2.00
-1.00
-9.00
0.00
-1.00
-3.00
-5.00
-7.00
0.00
2.00
4.00
6.00
constant action, $J_2$ ($10^{-6}$ m)
constant action, $J_1$ ($10^{-6}$ m)
7133A18

Fig. 7

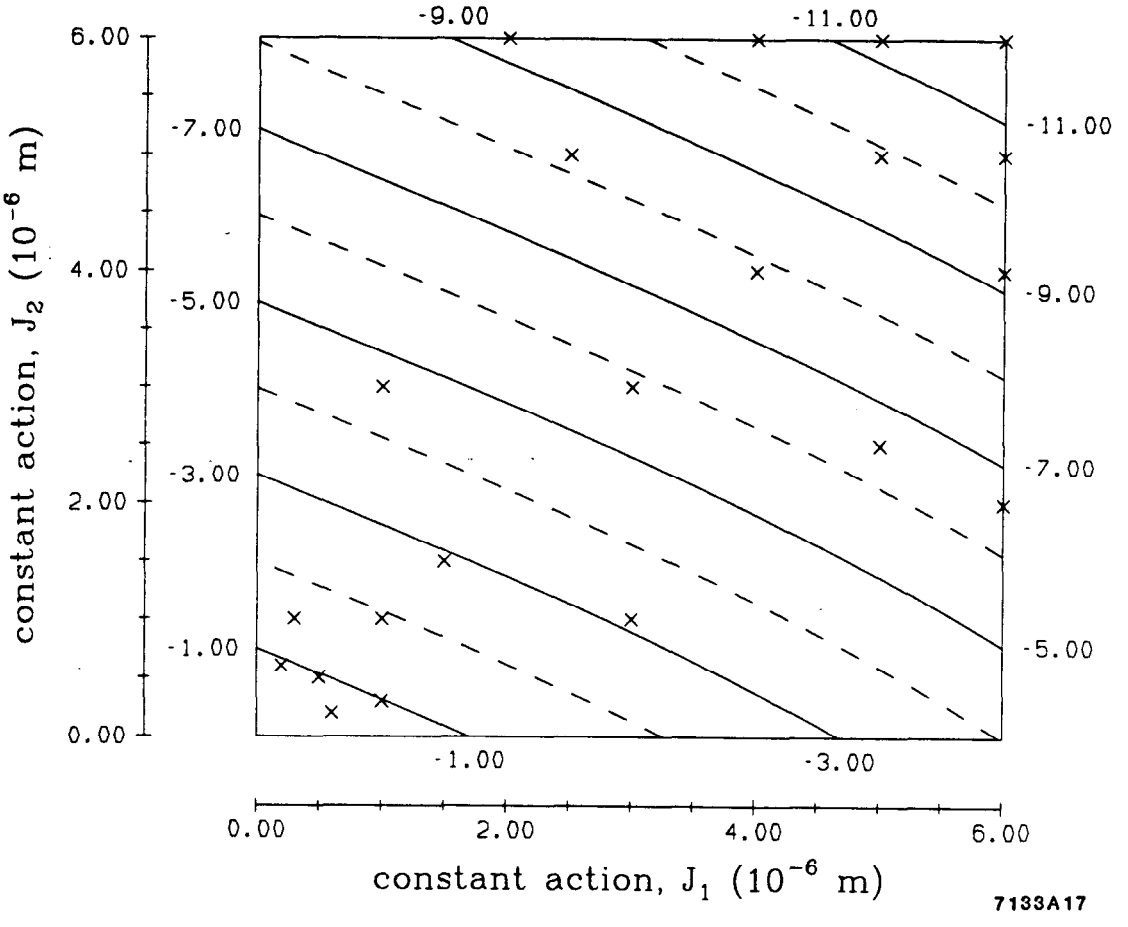
-9.00
-11.00
6.00
-7.00
-11.00
4.00
-5.00
-9.00
-3.00
-7.00
2.00
-1.00
-5.00
0.00
-1.00
-3.00
0.00
2.00
4.00
6.00
constant action, $J_2$ ($10^{-6}$ m)
constant action, $J_1$ ($10^{-6}$ m)
7133A17

Fig. 8

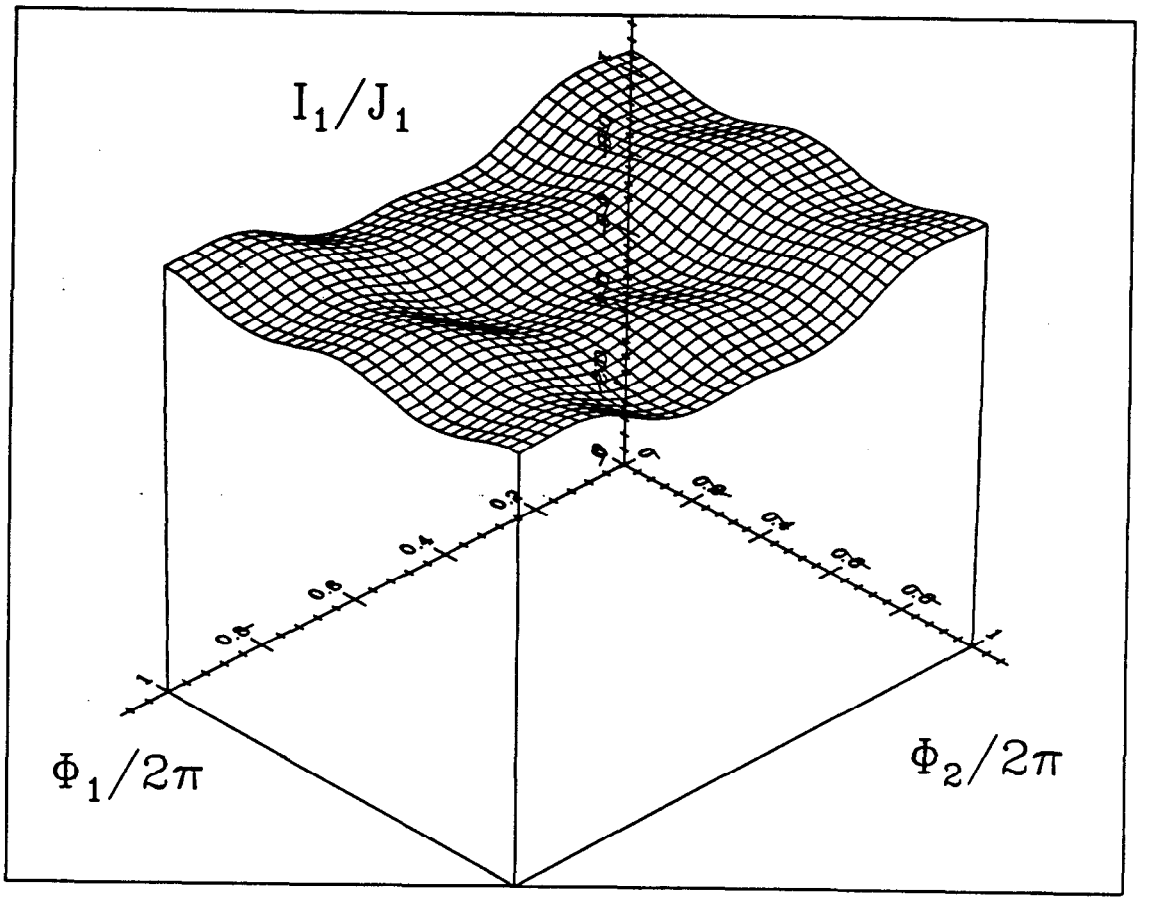


7133A7

Fig. 9

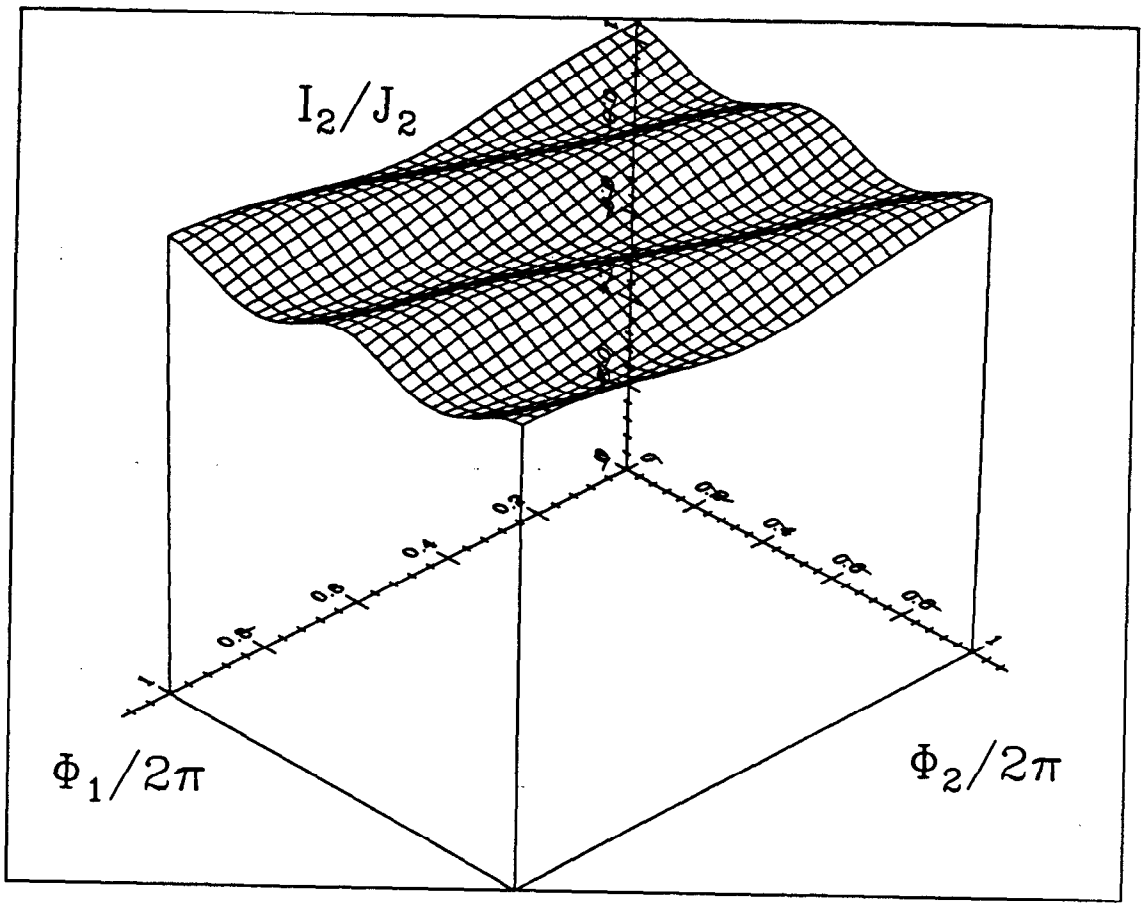


Fig. 10

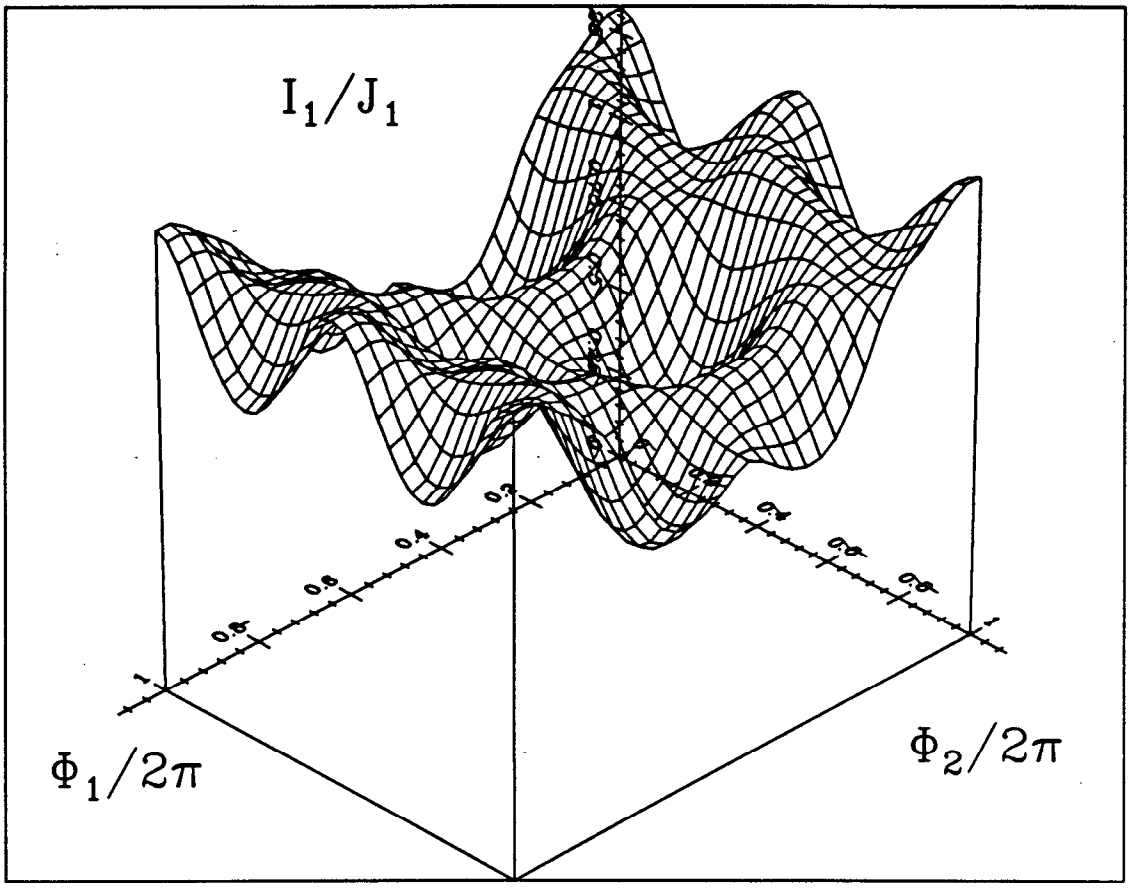


Fig. 11

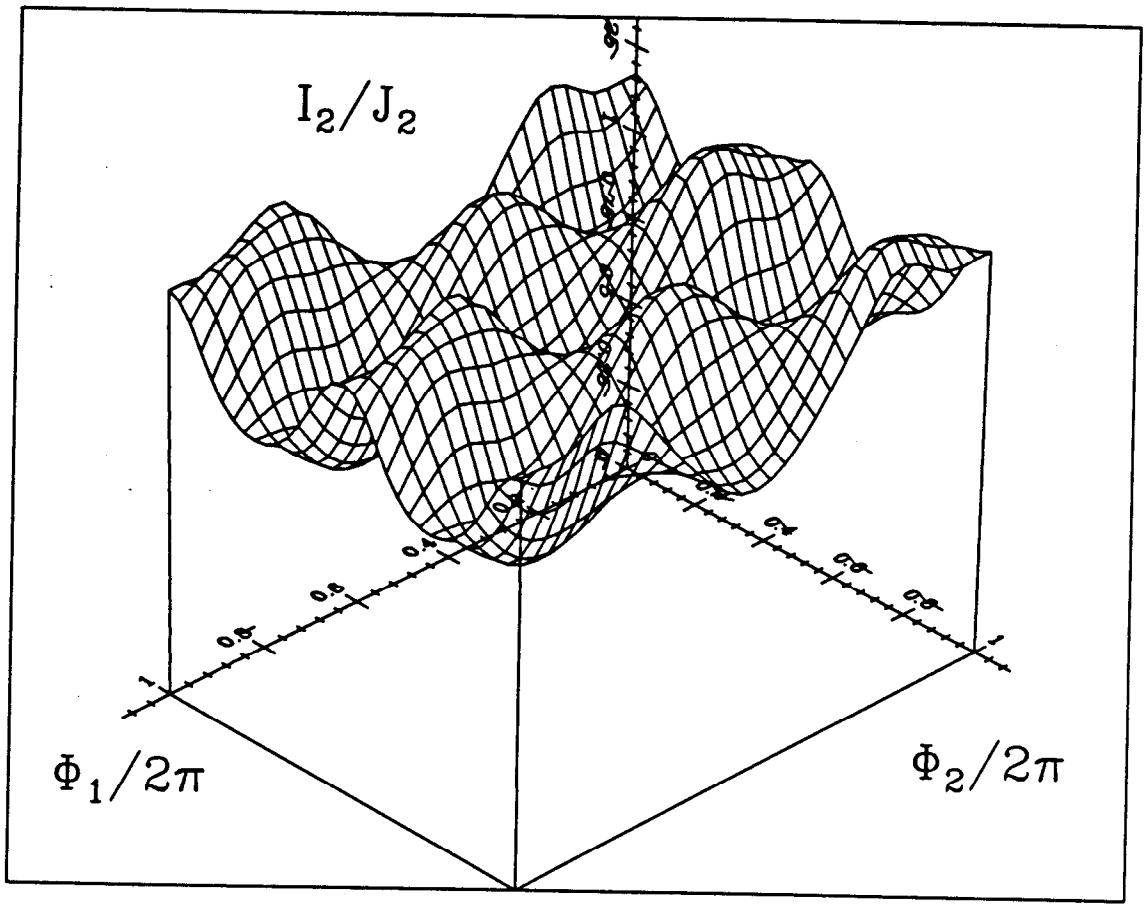


Fig. 12

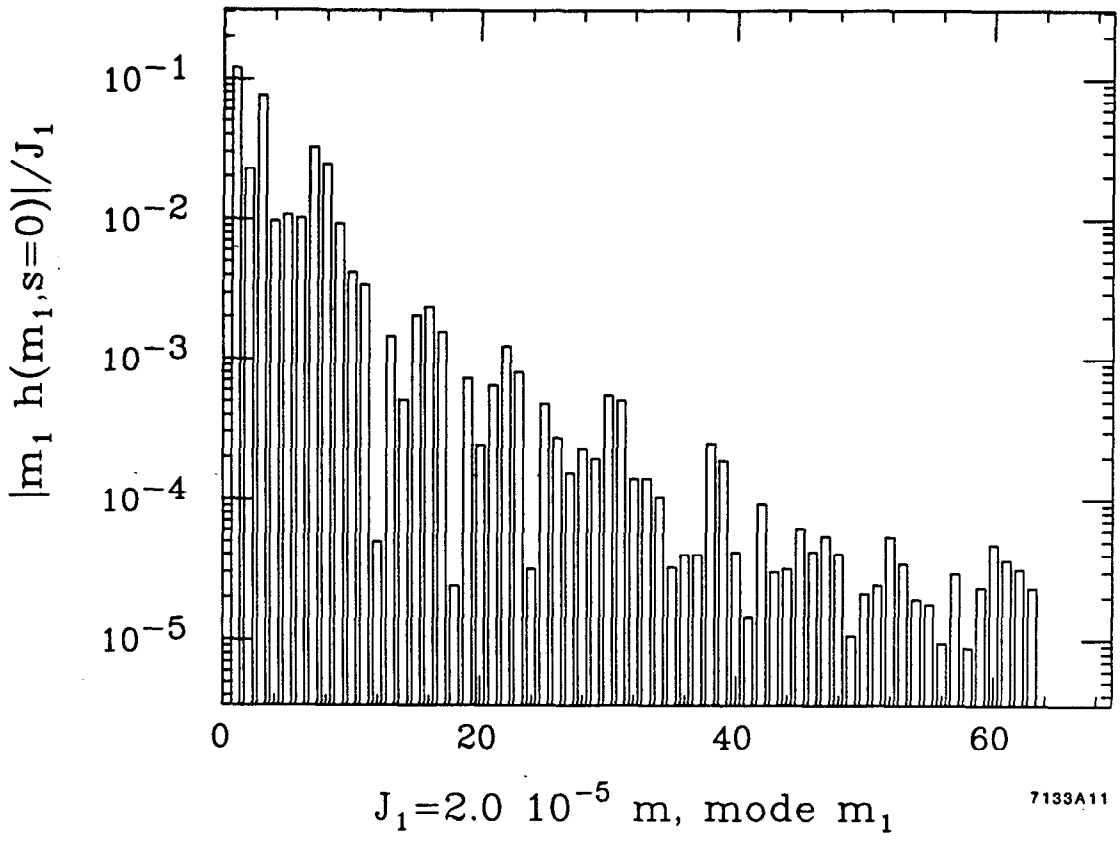
$|m_1\ h(m_1,s=0)|/J_1$
$10^{-1}$
$10^{-2}$
$10^{-3}$
$10^{-4}$
$10^{-5}$
0
20
40
60
$J_1$=2.0 $10^{-5}$ m, mode $m_1$
7133A11

Fig. 13

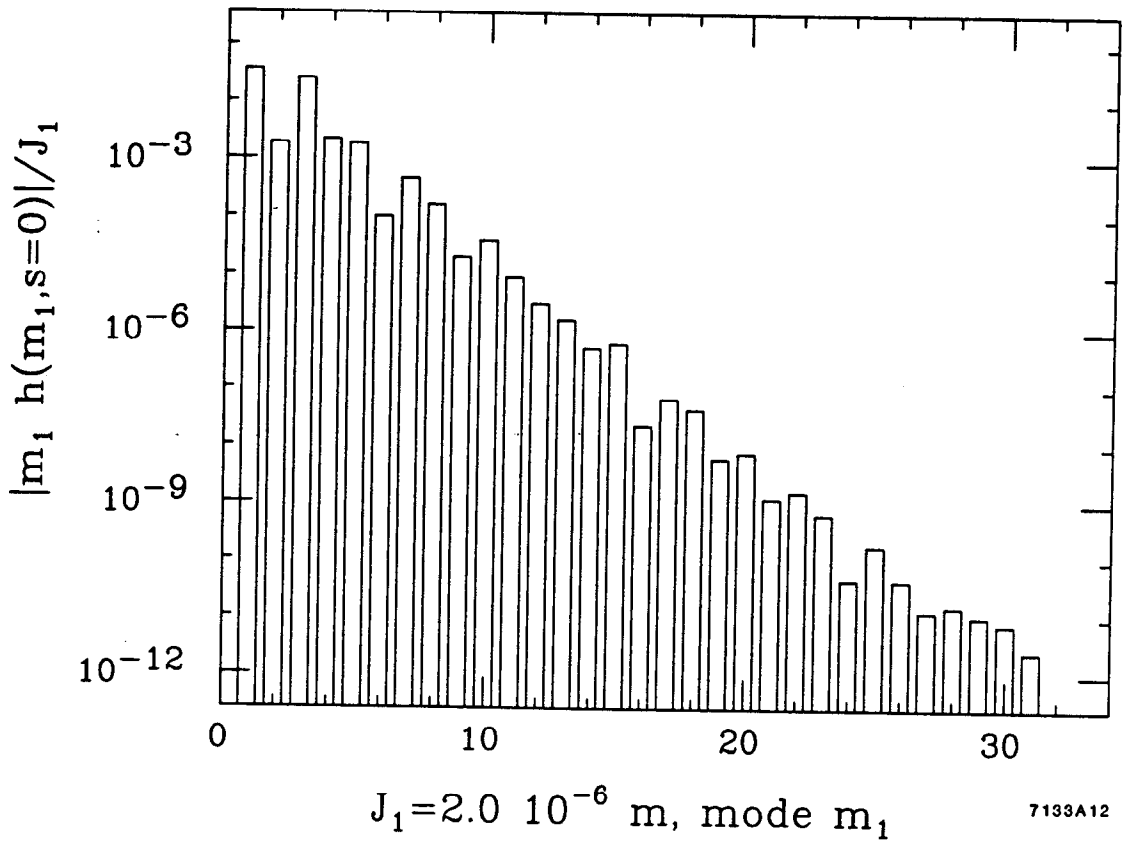
$|m_1\ h(m_1,s=0)|/J_1$
$10^{-3}$
$10^{-6}$
$10^{-9}$
$10^{-12}$
0
10
20
30
$J_1$=2.0 $10^{-6}$ m, mode $m_1$
7133A12

Fig. 14

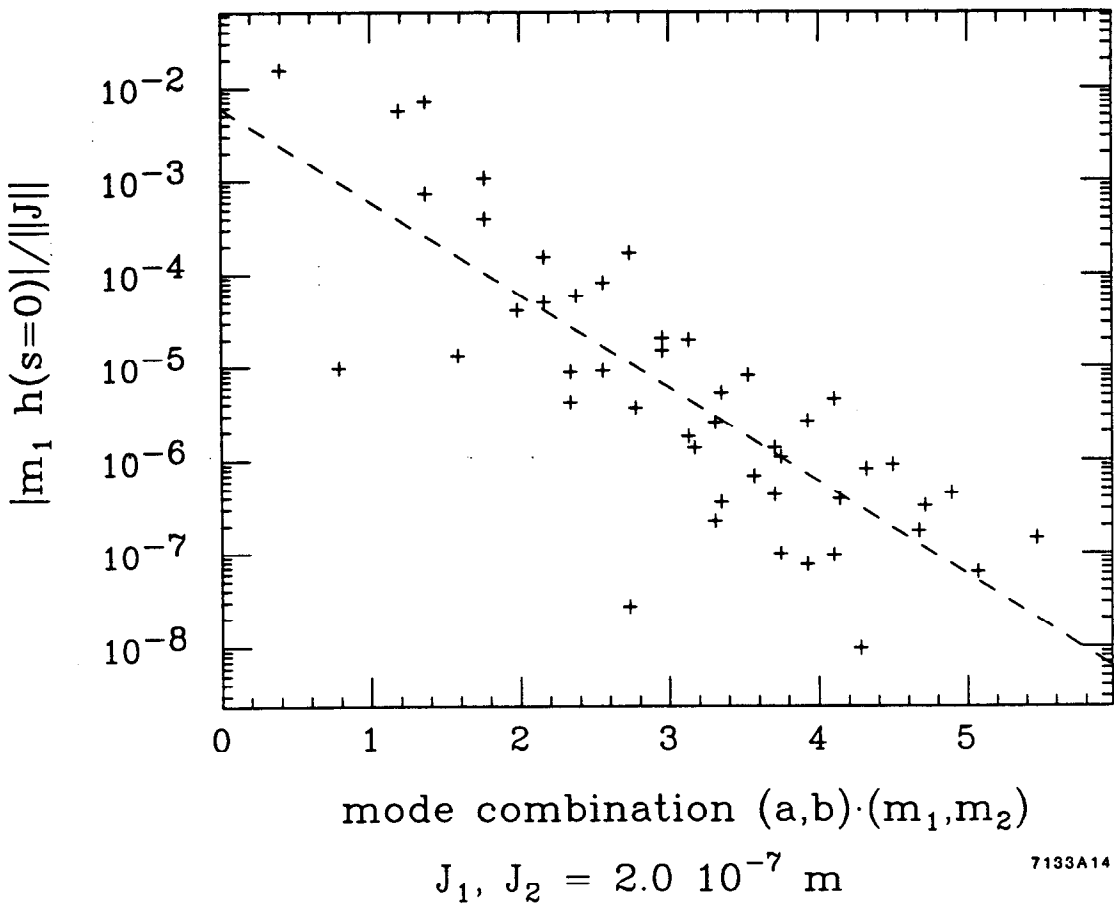
$10^{-2}$
$10^{-3}$
$10^{-4}$
$10^{-5}$
$10^{-6}$
$10^{-7}$
$10^{-8}$
$|m_1\ h(s=0)|/\|J\|$
0
1
2
3
4
5
mode combination $(a,b)\cdot(m_1,m_2)$
$J_1,\ J_2\ =\ 2.0\ 10^{-7}$ m
7133A14

Fig. 15

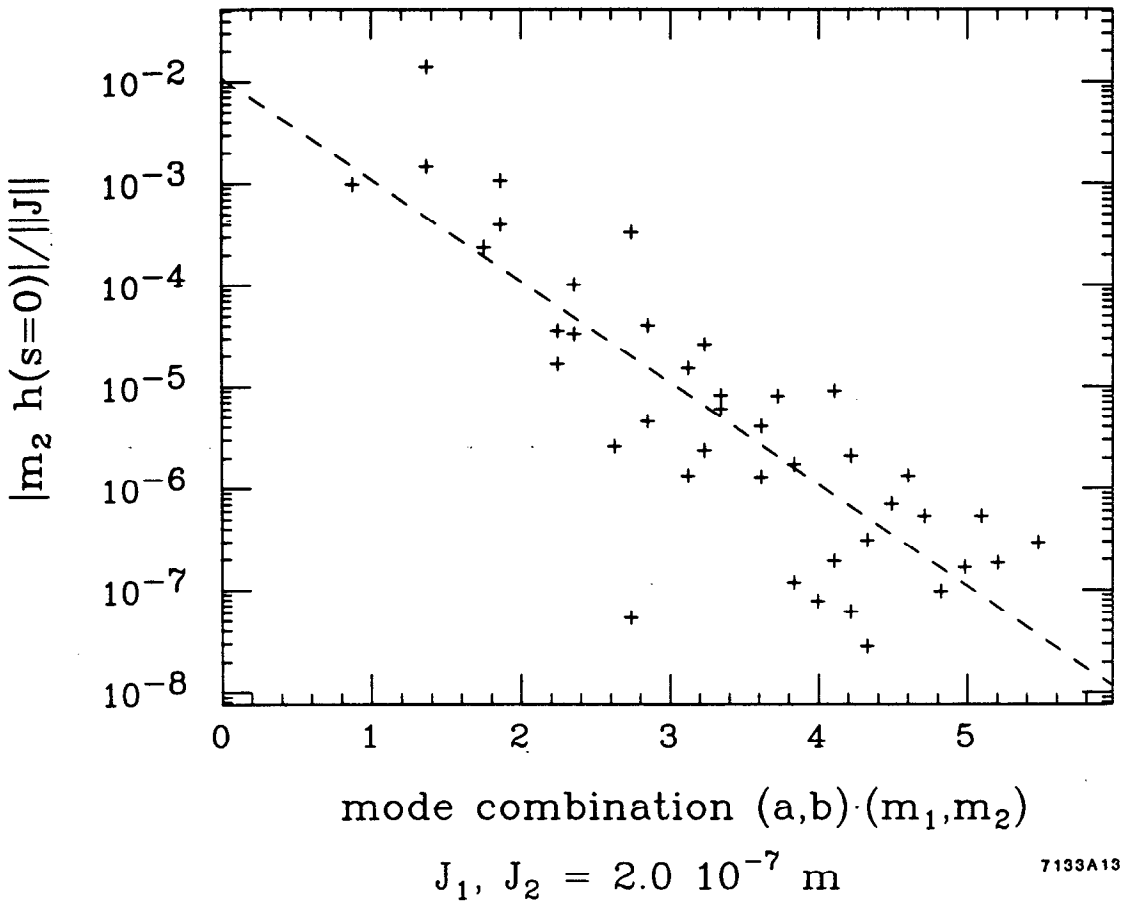
$|m_2\ h(s=0)|/||J||$
$10^{-2}$
$10^{-3}$
$10^{-4}$
$10^{-5}$
$10^{-6}$
$10^{-7}$
$10^{-8}$
0
1
2
3
4
5
mode combination (a,b)·$(m_1,m_2)$
$J_1,\ J_2 = 2.0\ 10^{-7}$ m
7133A13

Fig. 16

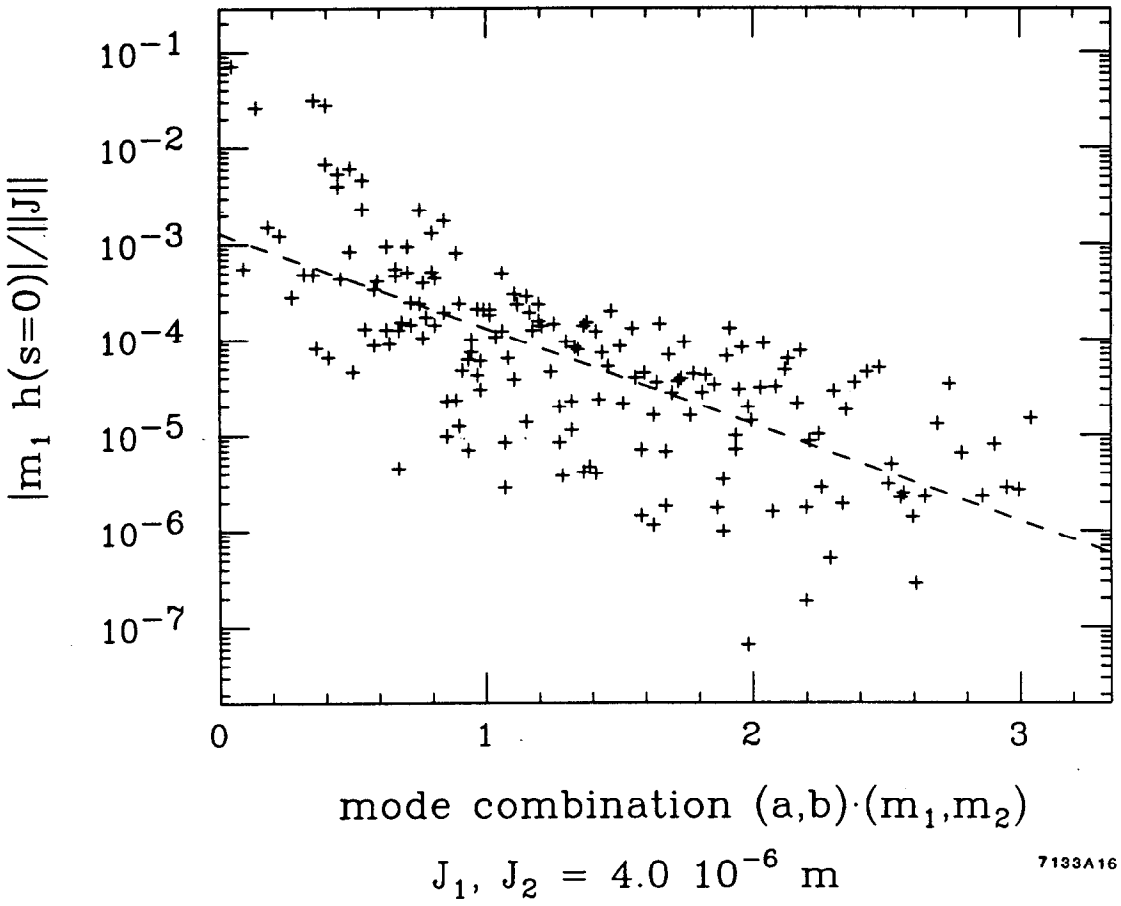
$10^{-1}$
$10^{-2}$
$10^{-3}$
$10^{-4}$
$10^{-5}$
$10^{-6}$
$10^{-7}$
$|m_1\ h(s=0)|/\|J\|$
0
1
2
3
mode combination $(a,b)\cdot(m_1,m_2)$
$J_1,\ J_2\ =\ 4.0\ 10^{-6}$ m
7133A16

Fig. 17

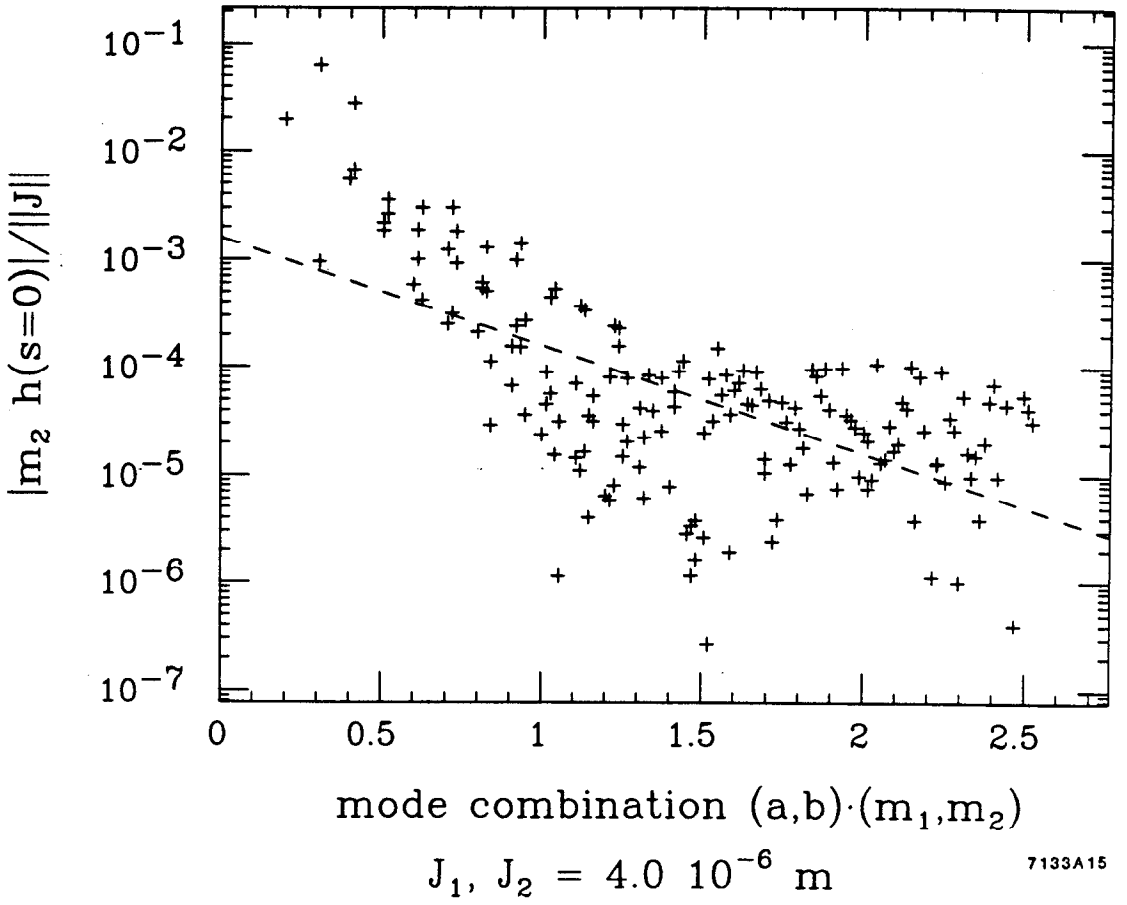
$10^{-1}$
$10^{-2}$
$10^{-3}$
$10^{-4}$
$10^{-5}$
$10^{-6}$
$10^{-7}$
$|m_2\ h(s=0)|/||J||$
0
0.5
1
1.5
2
2.5
mode combination $(a,b)\cdot(m_1,m_2)$
$J_1,\ J_2\ =\ 4.0\ 10^{-6}$ m
7133A15

Fig. 18